

# Pretrained battery transformer (PBT): A foundation model for battery life prediction

Ruifeng Tan<sup>1,2</sup>, Weixiang Hong<sup>1</sup>, Jia Li<sup>3\*</sup>, Jiaqiang Huang<sup>1,4,5\*</sup> and Tong-Yi Zhang<sup>6\*</sup>

<sup>1</sup>Guangzhou Municipal Key Laboratory of Materials Informatics and Sustainable Energy and Environment Thrust, The Hong Kong University of Science and Technology (Guangzhou), Nansha, Guangzhou, 511400, Guangdong, P. R. China.

<sup>2</sup>Department of Computer Science & Engineering, The Hong Kong University of Science and Technology, Clear Water Bay, Kowloon, 999077, Hong Kong, P. R. China.

<sup>3</sup>Guangzhou Municipal Key Laboratory of Materials Informatics and Data Science and Analytics Thrust, The Hong Kong University of Science and Technology (Guangzhou), Nansha, Guangzhou, 511400, Guangdong, P. R. China.

<sup>4</sup>Academy of Interdisciplinary Studies, The Hong Kong University of Science and Technology, Clear Water Bay, Kowloon, 999077, Hong Kong, P. R. China.

<sup>5</sup>Guangzhou HKUST Fok Ying Tung Research Institute, Nansha District, Guangzhou, 511458, Guangdong, P. R. China.

<sup>6</sup>Material Genome Institute, Shanghai University, 333 Nanchen Road, Shanghai 200444, P. R. China; Guangzhou Municipal Key Laboratory of Materials Informatics, Advanced Materials Thrust, and Sustainable Energy and Environment Thrust, The Hong Kong University of Science and Technology (Guangzhou), Nansha, Guangzhou, 511400, Guangdong, P. R. China.

\*Corresponding authors.

E-mails: [jjalee@ust.hk](mailto:jjalee@ust.hk); [seejhuang@hkust-gz.edu.cn](mailto:seejhuang@hkust-gz.edu.cn); [mezhangt@hkust-gz.edu.cn](mailto:mezhangt@hkust-gz.edu.cn)

## Abstract

Early prediction of battery cycle life is essential for improving battery design, manufacturing and deployment. However, despite encouraging progress with machine learning, battery life prediction remains constrained by scarce data and pronounced heterogeneity across battery chemistries, specifications, formation protocols and operating conditions. Although transfer learning has been widely explored to alleviate these challenges, its effectiveness is limited by the absence of a foundation model that can integrate heterogeneous battery life data and provide broadly useful knowledge for target-scenario specialization. Here we introduce the pretrained battery transformer (PBT), a foundation model for battery life prediction that incorporates battery-knowledge-encoded mixture-of-experts layers to learn from scarce and heterogeneous lifetime data. PBT is first pretrained on 13 lithium-ion battery datasets to yield a general PBT that encodes comprehensive battery lifetime knowledge, and is then adapted through transfer learning into specialized PBT models for target scenarios. Across 15 datasets covering 977 batteries and 528 sets of aging conditions from lithium-ion, sodium-ion and zinc-ion batteries, PBT achieves state-of-the-art performance, surpassing the strongest competing method by 21.9% on average, with gains of up to 86.9%. This study establishes, to our knowledge, the first foundation model for battery life prediction and provides a step towards shifting battery lifetime prediction from isolated, scenario-specific modelling tasks to a reusable knowledge foundation that can be specialized to target scenarios with limited data, with implications for other prediction problems characterized by scarce and heterogeneous data in sustainable energy.

## Introduction

Rechargeable batteries are central to the low-carbon energy transition, underpinning electric vehicles, grid storage and portable electronic devices<sup>1-5</sup>. In 2024, the global shipment of LIBs alone exceeded 1545 GWh, with total production projected to reach 4700 GWh by 2030<sup>6-8</sup>. In addition to LIBs, alternatives such as sodium-ion, zinc-ion and full-solid-state batteries are attracting attention because of their potential advantages in terms of cost and safety<sup>9-11</sup>. Nevertheless, all rechargeable batteries inevitably degrade because of the effects of intrinsic electrochemical processes<sup>12-14</sup>, leading to capacity fading, stability loss and safety concerns in practical applications<sup>13,15,16</sup>. Thus, aged batteries are retired from high-demand applications such as electric vehicles when they reach the end of their life cycle<sup>17-19</sup>. Battery lifetime is typically measured based on the number of charge–discharge cycles at which the battery capacity falls to 80% of the nominal capacity<sup>12,16</sup>. Traditionally, determining battery lifetime requires full-life cycling experiments that can take months or even years, creating a major bottleneck for battery development and evaluation<sup>13</sup>. Accurate early battery life prediction is therefore essential for optimizing battery design, production and utilization.

Data-driven methods have yielded impressive results for the early prediction of battery cycle life<sup>12,13,16,20-27</sup>. Early methods were based on features manually derived from voltage–current profiles<sup>16,22,25,27,28</sup>, physical models<sup>29</sup> or additional characterizations such as surface temperature<sup>24</sup> and electrochemical impedance spectrum<sup>30</sup>, which were then combined with machine learning methods. While these methods are effective with some datasets, they are validated under limited aging conditions and often depend on information or prior knowledge that may be unavailable or poorly transferable across battery specifications and usage profiles<sup>12,20,21,23</sup>, limiting their general applicability. A more generic alternative is to train neural networks directly on raw voltage–current signals, which are routinely recorded during cycling; such end-to-end models generally outperform feature-engineered approaches<sup>12,13,20,21,31,32</sup>. Among these neural network approaches, CyclePatch models<sup>13</sup> explicitly capture recurring cycle patterns in degradation tests, and achieve the best performance among 18 neural network models. Despite these advances, battery life prediction remains hindered by two fundamental challenges: the scarcity of lifetime data and the pronounced heterogeneity introduced by variations in cathode and anode materials, electrolytes, manufacturing processes, formation protocols and operating conditions<sup>12,13</sup>. In particular, data heterogeneity leads to variations in voltage–current profiles, producing distribution shifts between training

and testing data, a phenomenon known in machine learning as domain shift, which often degrades model performance<sup>5,33</sup>. Therefore, both data scarcity and heterogeneity must be considered in the design of practical battery lifetime prediction models.

Transfer learning has been widely explored to address data scarcity and heterogeneity in battery lifetime prediction. This approach is particularly helpful if different datasets share latent knowledge that can be transferred from source domains to target domains. Existing methods primarily fall into fine-tuning<sup>20,34</sup> and domain adaptation methods<sup>12,35</sup>. In fine-tuning methods, a model is first pretrained with data from source domains, and the model parameters are then fully or partially updated with information from target domains. For instance, Ma et al.<sup>20</sup> pretrained a neural network with 55 cells and fine-tuned it with information from 22 target cells subjected to held-out discharge protocols. By comparison, domain adaptation methods leverage information from both the source domain and the target domain during training to reduce the effect of domain shift and improve target-domain performance, often by learning domain-invariant or transferable representations. For instance, Zhang et al.<sup>35</sup> used domain-adversarial training to promote domain-invariant representations by constructing a domain classifier with gradient reversal mechanisms to reduce domain-specific information in the learned representations. Additionally, in a recent study<sup>12</sup>, BatLiNet was proposed based on the assumption that pairwise differences in feature representations correlate with pairwise differences in battery lifetime, and that this correlation is transferable across aging conditions; accordingly, the model incorporates inter-cell differences into learned representations. Despite encouraging results, existing transfer learning methods remain limited because they lack a general pretrained model that can integrate heterogeneous battery lifetime data and provide broadly useful knowledge for target-scenario specialization.

Foundation models (FMs) have emerged as pretrained models that encode general knowledge and can be adapted to diverse downstream applications through transfer learning<sup>36,37</sup>. These FMs exhibit broad utility and constitute indispensable components in many state-of-the-art natural language processing (NLP) and computer vision (CV) systems<sup>38-42</sup>. Nevertheless, the success of FMs hinges on architectures tailored to domain-specific data. For example, DeepSeek<sup>43,44</sup> and GPTs<sup>45,46</sup> employ transformer variants optimized for text, whereas CV FMs<sup>47-50</sup> use CNNs or vision transformers. However, effective architectures for encoding general battery lifetime knowledge are lacking. Specifically, experimental battery lifetime data are highly heterogeneous because battery degradation is shaped by diverse specifications, formation histories and operating conditions, spanning electrode/electrolyte materials<sup>58,60,6</sup>, chemistries<sup>13</sup>, cell formats<sup>13</sup>, formation protocols<sup>25,51</sup>, depths of discharge<sup>52-55</sup>, charge and discharge protocols<sup>20,52,54,56-59</sup>, stress factors<sup>53</sup> and operating temperatures<sup>53,55</sup>. At the same time, these datasets are limited in scale: even large single-scenario battery aging datasets typically contain only tens of batteries, and aggregated public lifetime datasets remain orders of magnitude smaller than the text and image corpora used to train general-purpose NLP and CV FMs. Building a battery FM for lifetime prediction therefore requires architectures that can organize heterogeneous lifetime information into a reusable knowledge foundation under data scarcity.

Here we present, to our knowledge, the first broadly transferable foundation model for battery cycle life prediction that operates directly on commonly available voltage–current data: the pretrained battery transformer (PBT). At its core is BatteryMoE, a mixture-of-experts layer that integrates battery knowledge through soft and hard encoders to guide learning under data scarcity while capturing shared knowledge across heterogeneous battery datasets and preserving specialization for distinct aging regimes. PBT is first pretrained on 13 lithium-ion battery datasets to construct a general PBT that encodes comprehensive battery lifetime knowledge, and is then adapted through transfer learning into specialized PBT models for target scenarios. Across 15 downstream datasets covering 977 batteries and 528 aging conditions, specialized PBT models achieve state-of-the-art performance across lithium-ion datasets represented in the pretraining data as well as sodium-ion, zinc-ion and large-format industrial lithium-ion datasets beyond the pretraining-covered specifications. Notably, competitive baseline neural networks pretrained on the same data do not achieve consistently positive transfer, even when adapted using the same transfer learning strategies,

highlighting the importance of domain-guided architectures for integrating heterogeneous battery lifetime data. Together, these results establish PBT as a practical battery foundation model that moves battery lifetime prediction beyond isolated, scenario-specific modelling by transforming heterogeneous aging data into reusable knowledge foundation for data-efficient specialization across various scenarios.

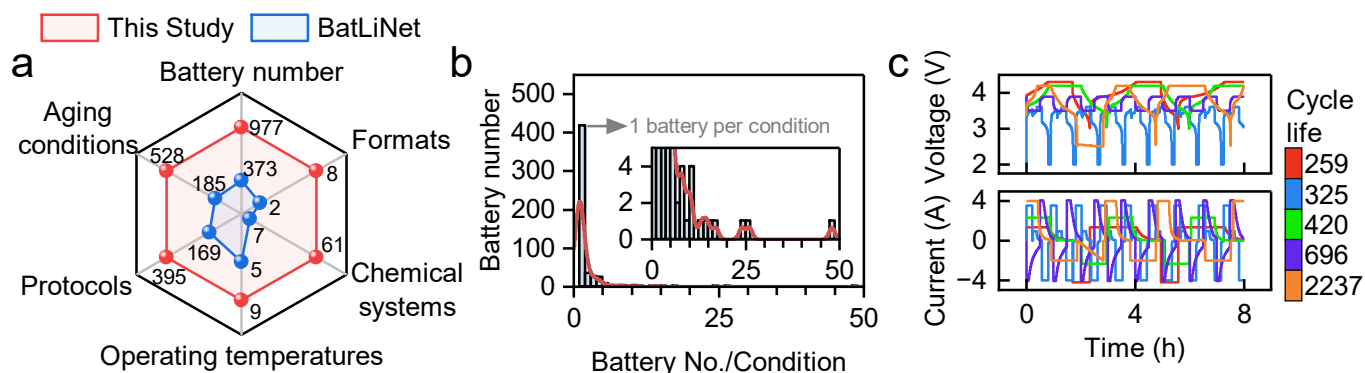


**Fig. 1 | Data used in this study and challenges arising from data scarcity and heterogeneity.** **a.** Comparison of data used in this study and those used in the second-largest battery cycle life prediction study (with BatLiNet<sup>12</sup>). Notably, both datasets were processed using the same pipeline (see Supplementary Note 1) and the filtered batteries were excluded from the statistical analysis<sup>13</sup>. In this work, we consider the battery format, anode, cathode, electrolyte, manufacturer, formation protocol, charge protocol, discharge protocols, and operating temperature as aging factors. Differences in these factors define distinct aging conditions. **b.** Distribution of the number of batteries across 528 aging conditions, showing that more than 400 aging conditions are represented by a single battery. **c.** Cycling patterns of five batteries under five aging conditions (see Supplementary Note 2) during the first eight hours of use.

## Datasets

To demonstrate the ability of the PBT to learn a widely transferable representation of battery life data, we compiled the largest and most diverse battery life database to date, consisting of 16 publicly available datasets<sup>13,15,16,20,25,51,53-56,58,60-63</sup> (see Supplementary Note 1 for the data preprocessing details and Supplementary Table 1 for the statistics of each dataset), including various formation protocols<sup>25,51</sup>, depths of discharge<sup>52-55</sup>, charge protocols<sup>15,16,52,54,55,58-60,64</sup>, discharge protocols<sup>20,52,54,56-59</sup>, stress factors<sup>53</sup>, materials<sup>56-58</sup>, operating temperatures<sup>53,55</sup>, chemistries of LIBs and other factors<sup>13</sup>. As shown in Fig. 1a, in comparison with the previous largest database<sup>12</sup>, our database includes 2.61 times batteries, 2.85 times aging conditions, 2.33 times charge–discharge protocols, 1.8 times operating temperatures, 8.71 times chemical systems, and 4 times physical formats.

Despite its unprecedented scale, our database still encodes data scarcity and heterogeneity challenges, as it contains information for only 977 batteries spanning 528 aging conditions, of which 418 are represented by single cells (Fig. 1b). Thus, the dataset provides a rigorous basis for evaluating the ability of the PBT to learn robustly in cases with data scarcity and heterogeneity.

## Overview of the pretrained battery transformer (PBT)

Our goal is to develop a unified FM for early cycle life prediction across a wide spectrum of early prediction settings<sup>12,21,24,32</sup> that can support a wide range of practically important scenarios, from battery screening and manufacturing evaluation to protocol design and deployment across diverse operating conditions. Given the first  $N$  charge–discharge cycles, with  $N$  being any integer  $\leq 100$ , the model predicts the cycle life—defined as the number of cycles at which the discharge capacity falls to 80% of the nominal capacity.

This problem is intrinsically difficult because battery life data are scarce and highly heterogeneous. Differences in materials, manufacturing processes, formation protocols and operating conditions can produce substantially different early-cycle behaviors and lifetime outcomes (Fig. 1c), making it difficult for conventional models to learn transferable pattern–lifetime relationships across datasets.

To address these challenges, we develop the pretrained battery transformer (PBT), with BatteryMoE as its core module—a neural component that embeds battery knowledge to guide learning across heterogeneous battery life data. In contrast to traditional approaches that rely on hand-crafted features,

dataset-specific assumptions or limited transfer mechanisms, BatteryMoE enables PBT to model diverse degradation behaviors by decomposing complex pattern–lifetime relationships into interpretable aspects informed by established battery knowledge, grouping batteries accordingly, and training a set of neural networks specialized for different groups. The outputs of the relevant neural networks are then aggregated to model the cycling behaviour of each battery. This design facilitates efficient learning across heterogeneous mappings while preserving aging-condition-specific knowledge, thereby improving both generalizability and transferability.

BatteryMoE comprises two main components: a battery-knowledge-encoded gate network (Battery gate) and a set of battery knowledge-informed expert networks (Fig. 2a). It builds on the mixture-of-experts (MoE) paradigm, which learns a gate network to route inputs to specialized neural networks (i.e., expert networks) and underlies many modern foundation models<sup>65</sup>. Conventional MoE architectures (Supplementary Fig. 1) rely solely on data-driven learning to assign input embeddings to experts, which can be ineffective for battery life prediction given limited data volume and complex voltage–current dynamics. To address this limitation, BatteryMoE injects battery knowledge through two complementary encoders, both validated by ablation studies (Supplementary Fig. 1). A soft encoder guides the gate network through knowledge-based pattern decomposition, producing more informative representations of cycling behaviors for expert routing. Complementing this, a hard encoder operates on the routing outputs of the soft encoder to impose physically meaningful constraints by filtering irrelevant expert networks through knowledge-based weight selection. Together, these two forms of knowledge injection couple flexible representation learning with structured expert selection, enabling BatteryMoE to learn transferable representations from scarce and heterogeneous aging data and forming the core of PBT.

The soft encoder (pink region in Fig. 2a) generates informative embeddings that replace direct voltage–current inputs to the gate network. Ten aging factors, dominating the cycling data patterns, were identified and grouped into three categories: specifications (e.g., cathode, anode, electrolyte, nominal capacity, format, and manufacturer), formation (e.g., formation protocol), and operation (e.g., charge protocol, discharge protocol, and temperature). Rather than rigidly embedding these factors as categorical or continuous variables, BatteryMoE employs a unified text-based template (Supplementary Fig. 2) that flexibly describes each aging condition. The completed templates are processed with an LLM-based aging embedder, which converts textual descriptions into vector representations. These vectors exhibit meaningful clustering patterns across batteries (Supplementary Fig. 3), reflecting the LLM’s prior knowledge of battery aging factors and facilitating downstream learning of their interactions. The resulting vector representations are then processed through a linear layer to produce the initial expert weights. Additional aging factors, such as stacking stress<sup>66</sup> and coating processes<sup>67</sup>, can be incorporated similarly, although they are not considered in this work because of their absence from the collected datasets.

The hard encoder imposes physically grounded routing constraints on the initial expert weights produced by the soft encoder, further reducing the complexity of model learning. We consider four key aging factors that can be categorized using well-established battery knowledge: cathode, anode, physical format and operating temperature. Other aging factors lack broadly accepted categorical definitions and are therefore not explicitly hard-coded here. For categorical factors—cathode, anode and format—BatteryMoE constructs specialized experts for each category, such as LFP and  $\text{Li}(\text{Ni}_x\text{Co}_y\text{Al}_{1-x-y})\text{O}_2$  (NCA) cathodes, and activates only those matching the input battery, because batteries sharing the same cathode, anode or format often exhibit related degradation behaviors<sup>55,68</sup>. With respect to temperature, which is treated as a continuous variable, experts are defined at discrete values and selected within  $\pm 5$  °C of the input, reflecting the fact that similar temperatures can induce similar degradation mechanisms<sup>69-71</sup>. For instance, in an 18650 LFP/graphite cell cycled at 25 °C, LFP, graphite, 18650-format, and 20–30 °C temperature experts are selected. In terms of implementation, the hard encoder is realized via knowledge-based weight selection, where the initial expert weights associated with nonmatching categories are filtered and removed, thereby enforcing physically meaningful routing. The selected experts operate in parallel to extract lifetime-relevant

representations, and their outputs are adaptively aggregated through learned weights. Notably, each category can have multiple experts to provide fine-scale specialization for aging factors that are not hard-coded (e.g., formation protocols and operating conditions), thus promoting accurate knowledge extraction and knowledge transfer across aging conditions. In this way, BatteryMoE alleviates the challenges associated with learning based on scarce and heterogeneous data by providing knowledge-guided inputs to the gate network and implementing physically grounded expert selection. This design enables the efficient capture and transfer of degradation knowledge across diverse battery systems. BatteryMoE also functions as a plugin module that is compatible with various neural architectures by allowing different network types to serve as experts.

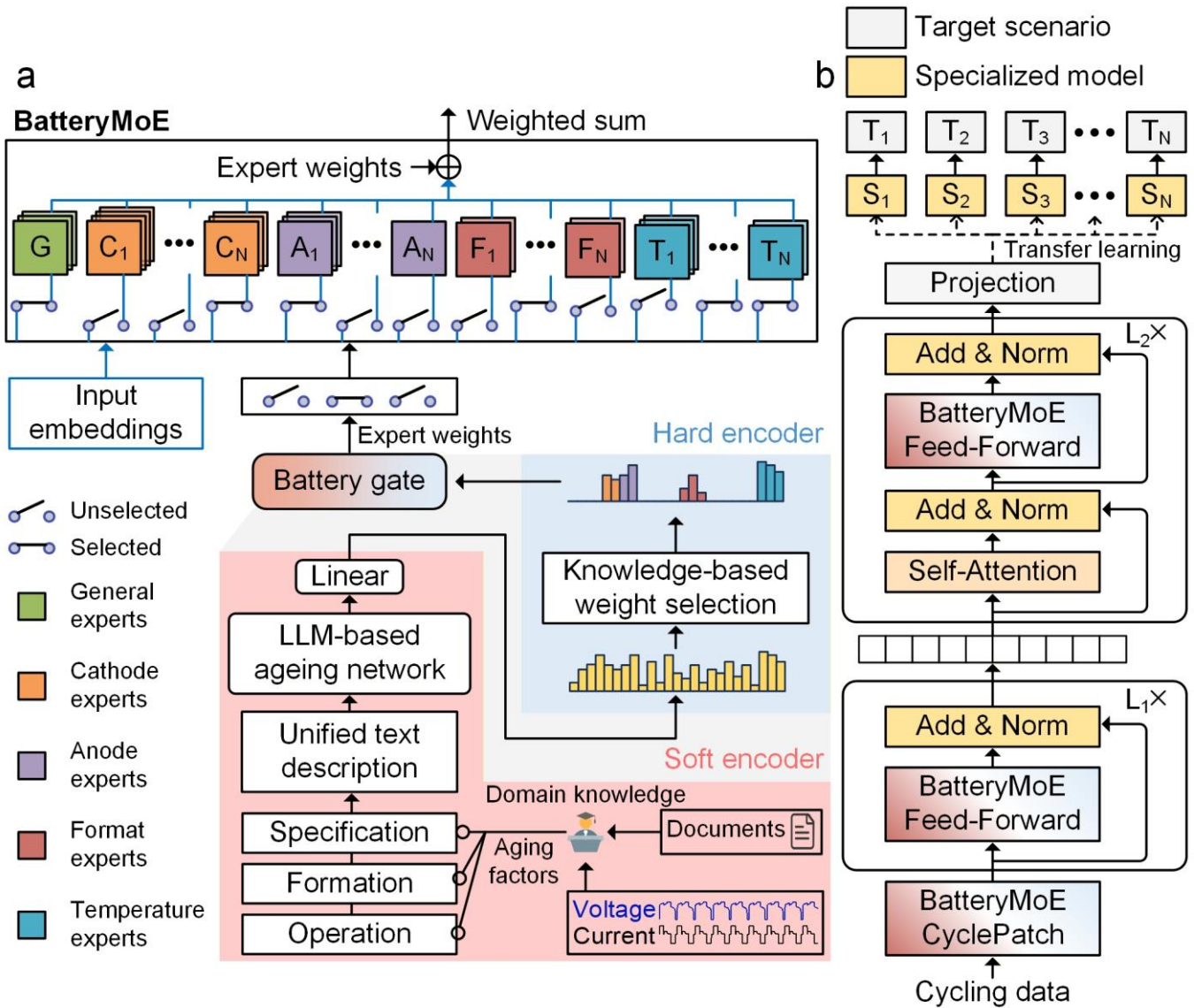


**Fig. 2 | Overview of BatteryMoE and the PBT.** **a.** Architecture of BatteryMoE. BatteryMoE comprises a battery gate and a set of expert networks. The battery gate integrates information from the soft and hard encoders to generate expert weights and route the input embeddings to the selected experts. The outputs of the selected experts are then aggregated using the learned expert weights. **b.** Data flow and overview of the architecture of the PBT.

As shown in Fig. 2b, we implement the PBT using BatteryMoE modules as the core computational units. The “BatteryMoE feedforward” module represents MoE networks selected according to BatteryMoE principles. In the PBT, each charge–discharge cycle is first encoded via “BatteryMoE CyclePatch”<sup>13</sup>, which tokenizes cycling data into cycle tokens. These embeddings are progressively refined through stacked

BatteryMoE feedforward layers with residual connections, producing higher-level representations that are passed to a transformer encoder, where standard feedforward layers are replaced by BatteryMoE modules. The encoder output is then projected to predict the battery cycle life.

In practical deployment, the pretrained model serves as a general PBT that encodes comprehensive battery lifetime knowledge from diverse aging scenarios and is adapted through transfer learning into a specialized PBT for a target application (Fig. 2b), such as lifetime prediction for batteries subjected to specific fast-charging or formation protocols.

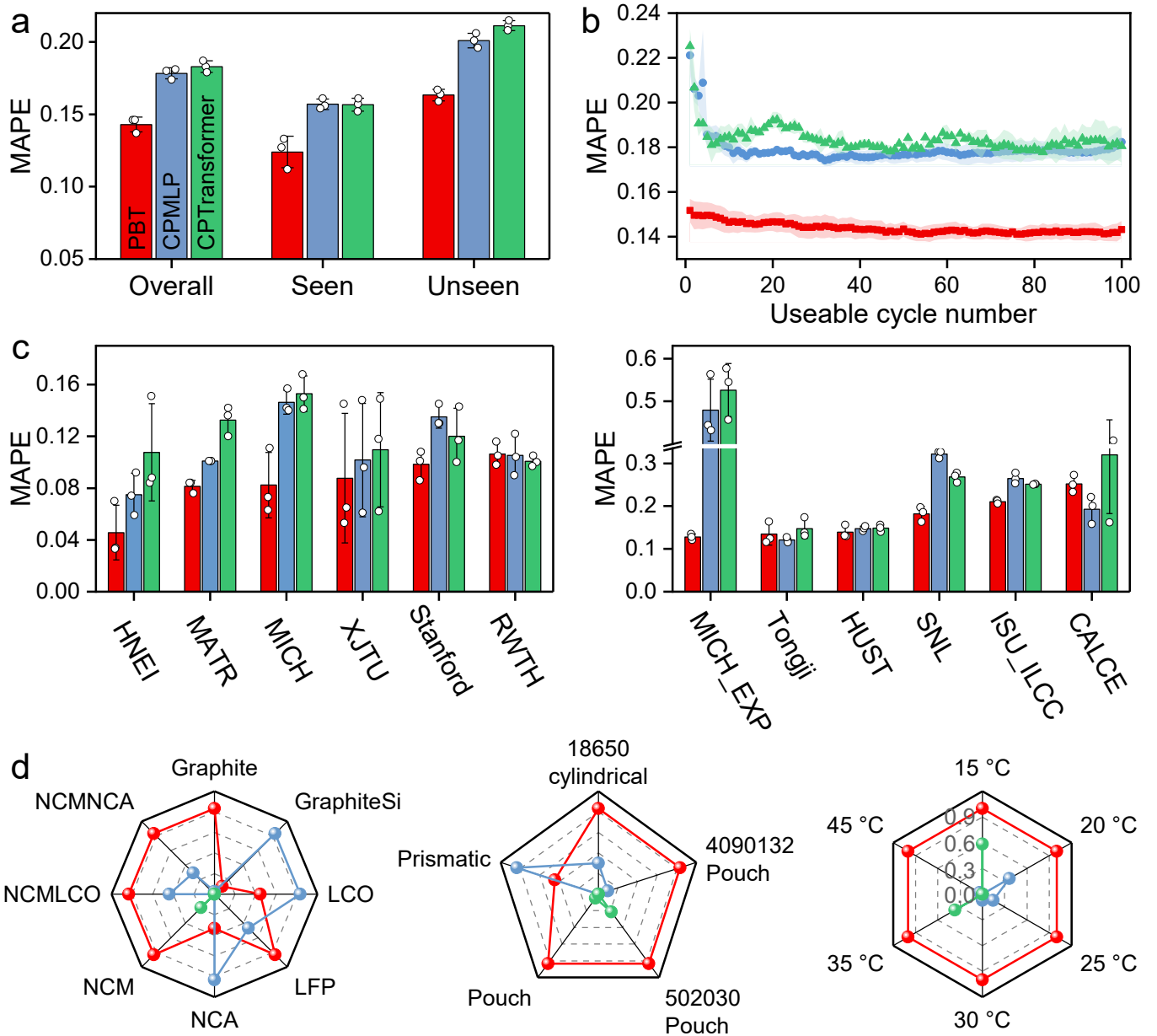


**Fig. 3 | Evaluations of the comprehensiveness of battery lifetime knowledge with the PBT.** **a.** Average mean absolute percentage error (MAPE) based on test sets from the 13 pretrained LIB datasets. “Overall” denotes the MAPE across all the batteries in the pretraining test sets. “Seen” and “Unseen” indicate the MAPE in cases with aging conditions that are included or not included in the training and validation sets of the pretraining data, respectively. **b.** Model performance with increasing numbers of useable cycles. The shaded areas represent standard deviations across three independent runs. **c.** Model performance based on the test sets from individual pretraining datasets. The error bars indicate the standard deviations of the mean. **d.** Model comparison based on chemistry, physical format and operating temperature. The radial values show the normalized MAPE computed as  $1 - (x - \min) / (\max - \min)$ , where  $x$  is the original MAPE and  $\min$  and  $\max$  are the best and worst MAPE, respectively, within each category. The red, blue and green colors denote the results of PBT, CPMLP and CPTransformer, respectively.

## Results

### Pretraining PBT to acquire comprehensive battery lifetime knowledge from diverse datasets

Pretraining provides an effective route to developing a transferable battery lifetime model by exposing it to degradation data collected across diverse aging scenarios before adaptation to specific downstream applications. In the PBT framework, the pretrained model constitutes a general PBT that encodes broadly useful battery lifetime knowledge from heterogeneous aging scenarios, whereas transfer learning adapts it

into a specialized PBT for a target application. The central question at this stage is therefore whether PBT can learn comprehensive and transferable representations from scarce yet heterogeneous battery lifetime data.

To address this question, we pretrained PBT on the training sets of 13 LIB datasets drawn from the abovementioned database. These datasets comprised 820 batteries spanning 418 aging conditions, 398 charge–discharge protocols, 8 operating temperatures, 15 chemical systems and 5 physical formats, covering most commercial LIB chemistries (see Supplementary Table 2 for the chemistries covered by each dataset). This broad coverage enables a systematic evaluation of whether PBT can extract lifetime-relevant knowledge across diverse battery specifications, protocols and degradation regimes. Each dataset was randomly split into training, validation and testing subsets at a 6:2:2 ratio. All model training was repeated three times with different random seeds, and the test sets were used to evaluate the knowledge acquired during pretraining. Note that the UL-PUR dataset included information for only 2 batteries after data preprocessing; therefore, no corresponding test set was established in this work. For all analyses, the mean absolute percentage error (MAPE) was employed as the evaluation metric because battery lifetime varies substantially across datasets (see Supplementary Fig. 4 for the battery life distributions from different datasets), ranging from 102 to 4999 cycles; thus, MAPE avoids bias associated with different lifetime scales. We compare the PBT against two baselines (CPMLP and CPTransformer) that were identified as the leading models among 18 neural networks<sup>13</sup>, including iTransformer<sup>72</sup>, PatchTST<sup>73</sup>, MICN<sup>74</sup>, and DLinear<sup>75</sup>. Both baselines employ CyclePatch<sup>13</sup> to generate cycle-level embeddings but differ in how they model inter-cycle relationships. CPMLP uses multilayer perceptrons to capture interactions across cycles, whereas CPTransformer leverages a transformer encoder. Because all models are trained on the same pretraining data, this comparison helps assess whether the BatteryMoE-based architecture enables PBT to capture more comprehensive pretraining knowledge than the baseline neural architectures.

First, we compare the overall results of the PBT with those of the leading baselines. As shown in Fig. 3a, PBT achieves the lowest MAPE, with an overall MAPE of 0.143, surpassing that of the second-best model (CPMLP) by 19.8%. To assess its robustness across data regimes, we further evaluate the performance under 61 seen and 56 unseen aging conditions, which correspond to in-distribution and out-of-distribution scenarios, respectively. The PBT outperforms the second-best model by 20.8% under seen conditions and 18.7% under unseen conditions, indicating that its superiority arises from consistent improvements for both in-distribution and out-of-distribution data. Moreover, we evaluate PBT across different numbers of useable cycles to examine how effectively the pretrained models extract useful information from the early operational data under different early prediction settings. PBT maintains clear advantages under all settings, achieving up to a 31.3% improvement when only information from the first cycle is available (Fig. 3b). Remarkably, when only the first cycle is provided as input, PBT with only the first cycle still outperforms the second-best model using 100 cycles, suggesting that the pretrained general PBT can make more effective use of limited early-cycle information than the baselines.

Next, we evaluate model performance on individual datasets. Because different datasets generally involve different battery specifications, protocols and degradation regimes, this analysis probes the breadth of lifetime knowledge captured by the pretrained models. PBT achieves the best results for 9 out of 12 datasets, with more than 20% MAPE improvements over the other methods for 8 datasets (Fig. 3c). For 3 datasets (RWTH<sup>62</sup>, Tongji<sup>58</sup>, and CALCE<sup>60,64</sup>), PBT does not yield the best performance, but it still performs on par with the best model for 2 of them (RWTH and Tongji). The deviation observed for the CALCE dataset is likely attributable to the absence of confidential aging factors, such as electrolyte configurations, stacking stresses and coating parameters, in the public data. This absence limits the ability of the model to fully resolve the underlying degradation processes. We posit that incorporating such proprietary information, which is often accessible to battery manufacturers, may further improve modelling accuracy. Overall, these results indicate that PBT captures broader pretraining knowledge across different battery datasets than the baseline models.

We further examine the comprehensiveness of the pretrained knowledge from three major sources of battery heterogeneity: chemistry, physical format and operating temperature. Specifically, we categorize batteries in the testing set along each perspective and report the MAPE for each category in Fig. 3d. PBT performs best for 5 out of 8 chemistries, 4 out of 5 physical formats and 6 out of 6 operating temperatures. Notably, PBT outperforms the second-best model by more than 13.7% for 15 of the 19 factors. These results suggest that PBT captures broader pretraining knowledge across diverse material systems, cell formats and thermal conditions than the baseline models.

Collectively, these pretraining evaluations show that the general PBT acquires more comprehensive battery lifetime knowledge from diverse LIB datasets than strong neural baselines trained on the same data. This provides a foundation for its application in various downstream cycle life prediction scenarios. Notably, these results assess the knowledge encoded in the pretrained general PBT, rather than the final performance expected in a target deployment scenario. In practical downstream applications, the general PBT is further adapted through transfer learning into a specialized PBT for a target application, as evaluated in the following sections.

### Building specialized PBT models for target scenarios within pretraining-covered battery specifications

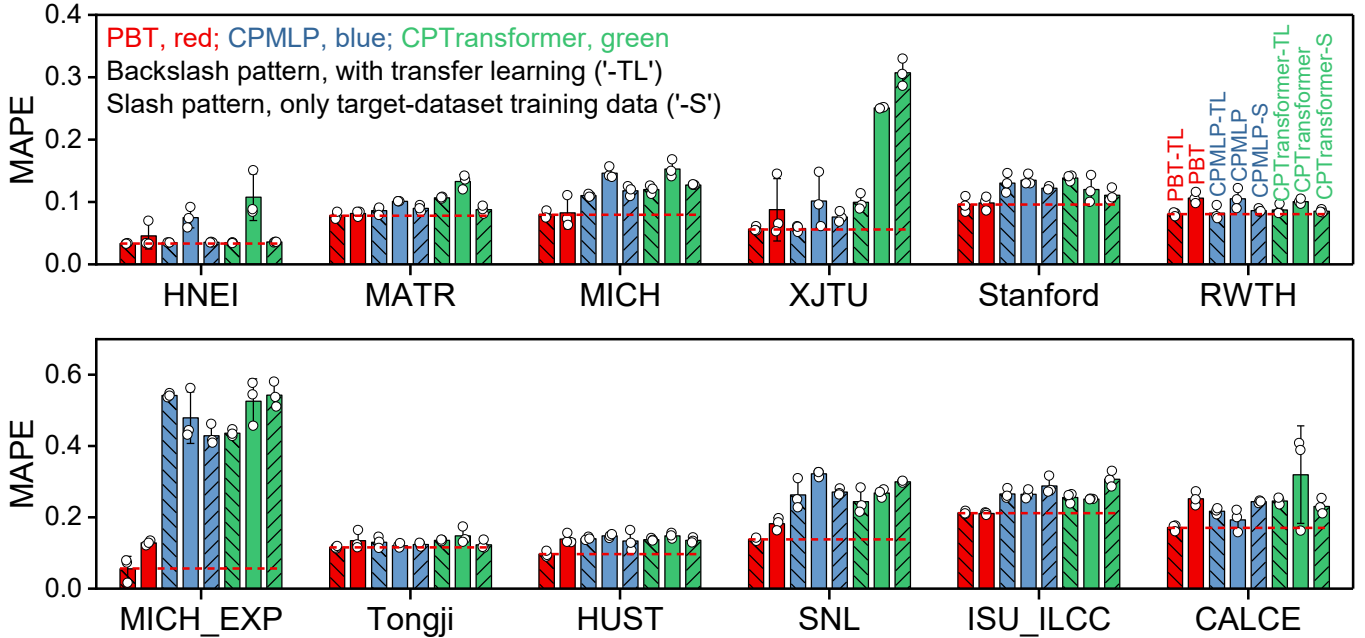


**Fig. 4 | Transfer-learning evaluation for specialized PBT models within pretraining-covered battery specifications.** The dashed lines indicate the performance of PBT-TL, as a visual reference. Transfer learning variants, denoted by the suffix -TL, are shown with a backslash pattern. Variants with the suffix -S represent models trained from scratch using only training data from the target dataset and are shown with a slash pattern. The error bars indicate the standard deviations across three independent runs.

Having established that the general PBT encodes comprehensive battery lifetime knowledge during pretraining, we next examine whether this knowledge can be adapted to build specialized PBT models for target scenarios whose battery specifications are covered by the pretraining data. We adapt PBT to 12 downstream datasets spanning different application settings using two common transfer learning strategies, fine-tuning and adapter tuning<sup>40</sup> (see Supplementary Note 3). These target datasets represent practically important scenarios, including fast-charging protocol optimization (MATR<sup>15,16</sup>), formation protocol analysis (Stanford<sup>51</sup>), cycle life evaluation under stress factors (MICH-EXP<sup>53</sup>), and lifetime prediction across diverse operating conditions (other datasets<sup>20,25,52,54-56,58-62</sup>). For a fair comparison, we apply identical transfer learning strategies to CPMLP and CPTransformer and report the best transfer learning results for each model in Fig. 4. We additionally include diagnostic comparisons with (i) direct inference using the

pretrained models without target-scenario adaptation and (ii) baseline models trained from scratch on each target dataset, thereby assessing the contributions of pretraining and transfer learning. PBT is also compared with BatLiNet<sup>12</sup>, a recently introduced transfer learning model for battery lifetime prediction (see Supplementary Note 4 for the implementation details).

As shown in Fig. 4, compared with CPMLP, CPTransformer and their transfer-learning variants, the specialized PBT obtained through transfer learning (PBT-TL) yields the lowest MAPE for all 12 datasets, achieving a greater than 10% improvement over other models for 8 of them and an average performance gain of 22.02% over the best baseline model. These results demonstrate the broad applicability of specialized PBT models across practical battery lifetime prediction scenarios within pretraining-covered battery specifications.

Notably, PBT-TL yields larger gains when target-scenario data are scarce and heterogeneous, particularly when limited training batteries span diverse aging conditions. Specifically, PBT-TL improves upon the best baseline by 3.85% for the HNEI dataset, which contains only 9 training batteries and 2 aging conditions; by 11.40% for the CALCE dataset, which contains only 9 training batteries and 4 aging conditions; and by 86.95% for the highly challenging MICH\_EXP<sup>53</sup> dataset, where each training battery is associated with a unique aging condition and only 7 batteries are available for training. Intriguingly, although the general PBT does not achieve the lowest MAPE on the CALCE dataset before target-scenario adaptation (Fig. 3c), the specialized PBT achieves state-of-the-art performance after transfer learning. This shift suggests that transfer learning enables PBT to adapt broadly learned degradation knowledge to CALCE-specific degradation patterns. It also underscores the importance of broad and relevant pretraining knowledge for building an effective battery foundation model. Moreover, because CPMLP/CPMLP-TL, CPTransformer/CPTransformer-TL and PBT/PBT-TL are trained on the same pretraining data and evaluated under the same transfer learning strategies, these results indicate that simply training neural models on diverse datasets is not sufficient to obtain broadly transferable battery lifetime representations. PBT addresses this challenge through the domain-guided routing and expert specialization of BatteryMoE, enabling effective knowledge transfer under data scarcity and heterogeneity.

The importance of transferable pretraining knowledge is further supported by the comparative transfer learning analysis. Although CPTransformer-TL outperforms CPTransformer on 10 datasets and CPMLP-TL outperforms CPMLP on 8 datasets, the frozen pretrained models (CPMLP and CPTransformer) and their variants trained from scratch using only target-dataset data (namely, those with the suffix -S in Fig. 4) achieve the second-best performance on 6 of the 12 datasets. This observation suggests that transfer learning alone can provide incremental improvements, whereas achieving state-of-the-art performance appears to depend on a pretrained model that encodes sufficiently relevant battery lifetime knowledge. This finding is further supported by the results of BatLiNet on the 12 datasets (Supplementary Table 3). BatLiNet does not match the performance of PBT-TL across all datasets and produces a MAPE  $\geq 50\%$  for 5 datasets with limited data or aging conditions substantially different from those of LFP/graphite batteries, a trend also noted in the original BatLiNet study<sup>12</sup>. Because the original BatLiNet model was trained solely with information from LFP/graphite batteries, we further evaluate BatLiNet using the PBT pretraining data to isolate the effect of pretraining data coverage. As summarized in Supplementary Table 4, simply enlarging BatLiNet's pretraining set in this way fails to improve its transfer performance for most datasets and may even degrade it, implying that integrating heterogeneous battery lifetime data is non-trivial. This outcome highlights both the difficulty and the necessity of developing an FM architecture that can effectively exploit diverse battery lifetime data, rather than merely relying on larger volumes of heterogeneous pretraining data.

In summary, these results show that the general PBT can be effectively adapted into specialized PBT models for target scenarios whose battery specifications are represented in the pretraining data. This

capability supports practical applications such as rapid lifetime assessment in manufacturing and the optimization of fast-charging and formation protocols within covered battery specifications.

### Building specialized PBT models for target scenarios beyond pretraining-covered battery specifications

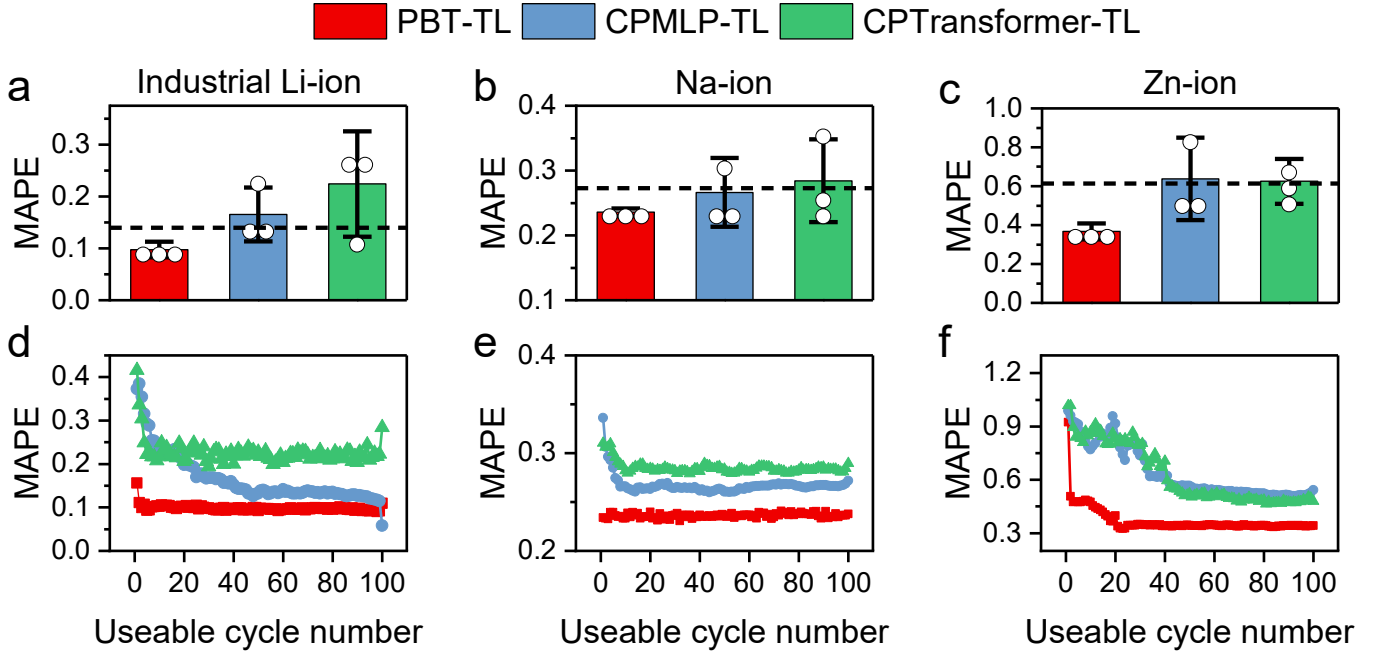


**Fig. 5 | Transfer-learning evaluation for specialized PBT models beyond pretraining-covered battery specifications.** a–c. Overall model performance based on the industrial Li-ion (a), Na-ion (b), and Zn-ion battery (c) datasets. The dashed lines indicate the best results obtained by the CPMLP and CPTransformer models trained from scratch using only the training data from the target dataset. The bars indicate the MAPE, and the error bars indicate the standard deviations across three independent runs. d–f. Model performance as a function of the number of useable cycles for the three datasets. In the industrial Li-ion dataset, 17 of 27 batteries do not include data from the 100<sup>th</sup> cycle, which causes an abrupt reduction in the number of evaluable batteries and may lead to a sudden change in MAPE.

A more stringent test of PBT is whether the general PBT can be adapted into specialized PBT models for target scenarios whose battery specifications fall outside the pretraining data. Such scenarios are particularly important for accelerating the development of next-generation batteries and industrial battery systems, where target chemistries or industrial cell designs may differ from those encountered during pretraining. We therefore evaluate whether the general PBT can be specialized on three out-of-distribution target datasets: sodium-ion (Na-ion), zinc-ion (Zn-ion) and large-format industrial Li-ion batteries. The Na-ion and Zn-ion datasets assess whether PBT can be specialized to chemistries beyond LIBs, whereas the industrial Li-ion dataset evaluates its applicability to high-capacity, large-format batteries relevant to real-world industrial development. For the industrial Li-ion dataset, we define the prediction target as the number of cycles at which the discharge capacity falls to 90% of the nominal capacity because most batteries in this dataset were not degraded to the 80% threshold. We compare PBT with the same baselines used in the previous section. Direct application of the general pretrained models yields unsatisfactory results because of substantial domain shifts; these results are therefore provided only as diagnostic comparisons and omitted from the main figure for clarity (Supplementary Table 5).

As shown in Fig. 5a–c, the specialized PBT obtained through transfer learning (PBT-TL) achieves the lowest MAPE for all three target datasets, outperforming the second-best model by 30.2%, 11.5% and 40.1% for the industrial Li-ion, Na-ion and Zn-ion battery datasets, respectively. These results demonstrate that the general PBT can be specialized through transfer learning to target applications involving both new battery chemistries and industrial-scale LIB development. The performance trends across varying numbers of useable cycles (Fig. 5d–f) further show that PBT-TL yields the best results in nearly all early prediction

settings, indicating that specialized PBT models maintain strong performance across different amounts of early-cycle information. Finally, BatLiNet does not match the performance of PBT-TL (Supplementary Tables 3–4). In addition, CPMLP-TL and CPTransformer-TL perform worse than models trained solely on the target datasets, suggesting that the gains of PBT-TL stem from its ability to adapt broadly learned battery lifetime knowledge to target scenarios beyond the pretraining distribution.

Collectively, these findings show that PBT can be adapted into specialized models even for target scenarios beyond pretraining-covered battery specifications. This capability extends the applicability of PBT from battery systems represented in the pretraining data to new chemistries and industrial battery designs, providing a basis for accelerating the development and deployment of next-generation energy storage materials and systems.

## Discussion and conclusions

This work introduces PBT, to our knowledge the first foundation model for battery cycle life prediction under data scarcity and heterogeneity. At the core of PBT is BatteryMoE, a battery-knowledge-guided mixture-of-experts module that enables effective learning from scarce and heterogeneous battery lifetime data. Through pretraining on 13 lithium-ion battery datasets, PBT first constructs a general PBT that encodes comprehensive battery lifetime knowledge. Transfer learning then adapts this general PBT into specialized PBT models for target scenarios across 15 datasets covering diverse practical applications, including different charge and discharge protocols, operating temperatures, stress factors, formation protocols, industrial battery designs and chemistries beyond lithium-ion systems. Notably, baseline neural networks pretrained on the same data do not achieve consistently positive transfer across these scenarios, even when adapted using the same transfer learning strategies, showing that broad transferability is not a trivial consequence of simply increasing the scale and heterogeneity of pretraining data. Together, these findings establish PBT as a practical battery foundation model that enables broadly learned degradation knowledge to be adapted into specialized lifetime prediction models across a wide spectrum of real-world scenarios.

Ablation and data scaling analyses clarify the factors that make PBT effective. Both the hard and soft encoders are essential for capturing underlying degradation behaviors (Supplementary Fig. 1), yielding significant performance gains. In addition, incorporating BatteryMoE consistently improves prediction accuracy across data scales (Supplementary Fig. 5), with gains comparable to those obtained by increasing the training set size by 33–50% for a baseline model, underscoring the value of the framework under data-scarce conditions. These results suggest that BatteryMoE is a domain-guided architecture that helps organize heterogeneous degradation knowledge into transferable and specialization-ready representations. Notably, the continued reduction in MAPE as more pretraining data are introduced further suggests that PBT has not yet saturated with respect to data scale. Together, these results show that the effectiveness of PBT arises from knowledge-guided architectural design and indicate that further expansion of high-quality pretraining datasets is a promising route towards more accurate and broadly transferable battery life prediction.

An important direction for future work is to extend PBT beyond battery-development-stage lifetime data to battery field data, such as data collected from energy storage systems<sup>4</sup> and electric vehicles<sup>3</sup>. A unified lifetime metric that is broadly accepted will be necessary to implement such an integrated approach, as batteries used in applications are typically operated under varying conditions with only partial charge–discharge data, making conventional cycle life calculations impractical. With such a metric, development and field data could be used complementarily, since both reflect degradation driven by related degradation modes<sup>69</sup>, even though their cycling patterns may differ. This integration could ultimately extend foundation models to encompass the entire battery lifecycle, from laboratory development to field operation. Such integration would allow battery foundation models to use large-scale operational data together with controlled laboratory data, thereby reducing the time and cost required to develop accurate models for

specific prediction scenarios. With sufficiently large and diverse pretraining data, future battery foundation models may further reduce the amount of target-scenario data required for specialization.

Beyond its specific implementation in PBT, BatteryMoE offers a scalable and flexible framework for incorporating battery knowledge into mixture-of-experts routing. In principle, the framework could be further extended to encode additional aging-related factors, such as electrolyte formulations or electrode coatings. More broadly, the two-level knowledge injection strategy in BatteryMoE, which combines a representation-guiding soft encoder with a constraint-imposing hard encoder, may provide a useful design pattern for other prediction problems characterized by data scarcity and heterogeneity, such as battery capacity estimation, solar cell lifetime prediction and wind power forecasting. In such settings, the soft encoder could incorporate domain-relevant factors, such as material composition, processing history and geographic position, whereas the hard encoder could introduce physically meaningful routing constraints derived from established governing factors. This perspective suggests that BatteryMoE is not limited to battery life prediction, but may offer a generalizable architecture for embedding domain knowledge into foundation models for a broader class of sustainable energy applications.

Overall, this study shows that tailored foundation models can provide an effective route to addressing the long-standing challenges of data scarcity and heterogeneity in battery life prediction. More broadly, it suggests that scientific machine learning for energy systems should move towards architectures that can structure fragmented experimental observations into transferable, specialization-ready representations. In this sense, battery life prediction provides a representative example of how domain knowledge can guide foundation-model design and make scarce and heterogeneous experimental data more reusable across sustainable energy applications.

## Methods

The pretrained battery transformer (PBT) is implemented as a battery-knowledge-encoded neural architecture with BatteryMoE as its core module. As illustrated in Fig. 2b, PBT consists of a BatteryMoE-CyclePatch layer, a BatteryMoE intra-cycle encoder with  $L_1$  layers, a BatteryMoE-inter-cycle encoder with  $L_2$  layers, and a projection head. We first describe BatteryMoE, followed by the individual model components.

**BatteryMoE.** BatteryMoE is a mixture-of-experts layer that incorporates battery knowledge through a soft encoder and a hard encoder. The soft encoder represents predefined aging factors that dominate cycling data patterns, whereas the hard encoder imposes routing constraints based on well-established categorical or continuous aging factors. These factors—spanning battery specifications, formation and operation—are embedded into vectors as follows:

$$\mathbf{e} = E_{ae}(\text{specification, formation, operation}), \quad (1)$$

where  $E_{ae}$  denotes an aging embedder and  $\mathbf{e}$  is the resulting vector representation. To construct a universal embedder applicable to arbitrary combinations of aging factors, we devise a large language model (LLM)-based aging embedder that produces token embeddings from a textual prompt describing the factors:

$$\bar{\mathbf{E}} = LLM(\text{prompt}), \quad (2)$$

$$\mathbf{e} = \text{lastValid}(\bar{\mathbf{E}}), \quad (3)$$

where prompt (Supplementary Fig. 2) is a text description of the aging factors,  $\bar{\mathbf{E}} \in \mathbb{R}^{L \times d_{LLM}}$  is the embedding of tokens obtained from the prompt, and  $\mathbf{e} \in \mathbb{R}^{d_{LLM}}$  is the embedding of the last valid token in  $\bar{\mathbf{E}}$ . The embedding of the final valid token  $\mathbf{e}$  is used as the aging-condition representation because, under causal attention, this token can attend to the preceding tokens in the prompt. In the present study, Llama-

3.1-8b-Instruct<sup>76</sup> is used as the LLM to embed the prompt. The LLM parameters are frozen during PBT training to avoid overfitting and training instability when only limited training data are available. A nonlinear transformation is then applied to obtain informative representations:

$$\hat{\mathbf{e}} = \text{LeakyReLU}(\mathbf{W}\mathbf{e} + \mathbf{b}), \quad (4)$$

where  $\mathbf{W} \in \mathbb{R}^{d_{ff} \times d_{LLM}}$  and  $\mathbf{b} \in \mathbb{R}^{d_{ff}}$ . The processed embedding  $\hat{\mathbf{e}}$  is shared across BatteryMoE layers and used in a distinct linear layer of each BatteryMoE layer to determine expert weights as follows:

$$\mathbf{g} = [g_1, g_2, g_3, \dots, g_{K_s}] = \mathbf{W}_2 \hat{\mathbf{e}} + \mathbf{b}_2, \quad (5)$$

where  $\mathbf{g} \in \mathbb{R}^{K_s}$  is the initial unnormalized expert weights for  $K_s$  expert networks,  $\mathbf{W}_2 \in \mathbb{R}^{K_s \times d_{ff}}$  and  $\mathbf{b}_2 \in \mathbb{R}^{K_s}$  are learnable parameters and  $K_s$  is the number of specialized expert networks in a BatteryMoE layer.

The hard encoder (blue in Fig. 2a) imposes knowledge-based routing constraints within the MoE layer. We apply hard routing to four aging factors with well-defined categories or physically interpretable ranges across the collected datasets: cathode, anode, physical format and operating temperature. Other factors, such as formation and charge protocols, are not hard-coded because their categorical definitions are less clear across studies. Under this scheme, only the expert weights associated with the matching categories or temperature range are retained for modeling a given battery:

$$\tilde{\mathbf{g}} = \sigma(\mathbf{g}), \quad (6)$$

$$\bar{\mathbf{g}} = [\bar{g}_1, \bar{g}_2, \bar{g}_3, \dots, \bar{g}_{K_s}] = \frac{\tilde{\mathbf{g}}}{\sum \tilde{\mathbf{g}}} \quad (7)$$

where  $\sigma(\cdot)$  denotes the knowledge-based weight selection mechanism used to set irrelevant expert weights to zero, and  $\bar{\mathbf{g}}$  is the resulting normalized expert-weight vector used in BatteryMoE to aggregate outputs of expert networks. Specifically, for categorical factors (cathode, anode, and physical format), only expert networks corresponding to the selected category are used. For temperature, which is treated as a continuous variable, experts whose specialized temperatures fall within  $\pm 5$  °C of the input are selected. The resulting knowledge-informed expert weight  $\bar{\mathbf{g}}$  is the output of the battery gate (Fig. 2a) and is subsequently used to aggregate outputs from expert networks:

$$\mathbf{M}^l = \sum_{i=1}^{K_g} F_i(\mathbf{M}^{l-1}) + \sum_{j=1}^{K_s} \bar{g}_j F_{j+K_g}(\mathbf{M}^{l-1}), \quad (8)$$

where  $K_g$  denotes the number of general experts and  $F_i(\cdot)$  is an expert network. This formulation makes BatteryMoE a plug-and-play component compatible with various expert architectures  $F(\cdot)$ . For brevity, in the following subsections, we refer to a BatteryMoE layer as BatteryMoE( $F(\cdot)$ ) when  $F(\cdot)$  is used as the expert network architecture. To ensure effective expert specialization, each category is assigned one expert for up to 100 batteries in the training set, with an additional expert added for every subsequent 100, following a round-to-the-nearest-hundred rule (e.g., 151  $\rightarrow$  two experts, 101  $\rightarrow$  still one expert). This adaptive allocation scheme supports fine-scale specialization through data-driven learning for categories with abundant training data.

**BatteryMoE-CyclePatch.** Motivated by the previous success of CyclePatch<sup>13</sup>, BatteryMoE-CyclePatch is employed to patch the cycling data for each cycle into a token. Let  $\mathbf{X}_{1:S} \in \mathbb{R}^{(300 \times S) \times 3}$  denote the voltage, current and capacity sequence of the first  $S$  cycles (each cycle is resampled to 300 data points; see Supplementary Note 5). The process of BatteryMoE-CyclePatch can be described as follows:

$$[\mathbf{X}_1, \mathbf{X}_2, \mathbf{X}_3, \dots, \mathbf{X}_S] = \text{Segment}(\mathbf{X}_{1:S}), \quad (9)$$

$$\widehat{\mathbf{X}}_i = \text{BatteryMoE}\left(\text{Linear}(\text{Flatten}(\mathbf{X}_i))\right), \quad (10)$$

where  $\mathbf{X}_i \in \mathbb{R}^{300 \times 3}$ ,  $\text{Flatten}(\mathbf{X}_i) \in \mathbb{R}^{900}$ , and  $\text{Linear}(\cdot)$  is a linear layer that projects  $\text{Flatten}(\mathbf{X}_i)$  to  $\widehat{\mathbf{X}}_i \in \mathbb{R}^d$ . In this context, the recurring cycling data patterns are explicitly segmented into distinct tokens  $\widehat{\mathbf{X}} = [\widehat{\mathbf{X}}_1, \widehat{\mathbf{X}}_2, \dots, \widehat{\mathbf{X}}_S]$ .

**BatteryMoE-Intra-cycle encoder.** Following CyclePatch, an intra-cycle encoder is employed to mine useful high-level representations for each cycle. This process for one intra-cycle encoder layer can be formulated as follows:

$$\mathbf{H}_i^l = \text{LN}\left(\text{BatteryMoE}\left(\text{FFN}(\mathbf{H}_i^{l-1})\right) + \mathbf{H}_i^{l-1}\right), \quad (11)$$

where  $\text{LN}(\cdot)$  denotes layer normalization<sup>77</sup>,  $\text{FFN}(\cdot)$  is a feedforward network with a GELU<sup>78</sup> activation function,  $\mathbf{H}_i^l \in \mathbb{R}^d$ , and  $\mathbf{H}_i^0 = \widehat{\mathbf{X}}_i$ . Stacking  $L_1$  layers intra-cycle encoder layers produces cycle-token embeddings for the first  $S$  cycles, producing  $\mathbf{H}^{L_1}$ , and input  $\mathbf{H}^{L_1}$  into the inter-cycle encoder to model critical information across cycles. For efficient batch operation, all  $\mathbf{H}^{L_1}$  vectors are zero-padded to a length of 100, which is the largest useable cycle number for the model input. Therefore,  $\mathbf{H}^{L_1} \in \mathbb{R}^{100 \times d}$ .

**BatteryMoE-Inter-cycle encoder.** The inter-cycle encoder adopts a transformer<sup>79</sup> encoder framework for modeling information across cycle tokens. First, positional encoding is used to incorporate position information into the intra-cycle encoder output:

$$\bar{\mathbf{H}}^{L_1} = \text{PE}(\mathbf{H}^{L_1}) + \mathbf{H}^{L_1}, \quad (12)$$

where  $\text{PE}(\cdot)$  is the positional encoding introduced in the original transformer paper<sup>79</sup>. Then,  $\bar{\mathbf{H}}^{L_1}$  is input into the inter-cycle encoder, where the process for one layer is as follows:

$$\mathbf{P}^l = \text{LN}(\text{Attention}(\mathbf{P}^{l-1}, \mathbf{P}^{l-1}, \mathbf{P}^{l-1}) + \mathbf{P}^{l-1}), \quad (13)$$

$$\mathbf{U}^l = \text{LN}\left(\text{BatteryMoE}\left(\text{FFN}(\mathbf{P}^l)\right) + \mathbf{P}^l\right), \quad (14)$$

where  $\text{Attention}(\cdot, \cdot, \cdot)$  is the self-attention<sup>79</sup> operation,  $\mathbf{P}^0 = \bar{\mathbf{H}}^{L_1}$ , and  $\mathbf{U}^l \in \mathbb{R}^{100 \times d}$  is the output of the  $l^{\text{th}}$  inter-cycle encoder layer. Note that the attention mask is adopted to ignore the padded tokens in  $\text{Attention}(\cdot, \cdot, \cdot)$ .

**Projection head.** After the intra-cycle and inter-cycle encoders, the resulting sequence representation  $\mathbf{U}^{L_2}$  contains both intra-cycle and inter-cycle information. The last nonmasked vector in  $\mathbf{U}^{L_2}$  is denoted by  $\mathbf{z}$  and is used as the input to the projection head. The final prediction  $\hat{y}$  can be produced via a projection head that employs a mixture of linear layers:

$$\mathbf{g} = [g_1, g_2, g_3, \dots, g_{K_S}] = G(\mathbf{z}), \quad (15)$$

$$\hat{y} = \sum_{i=1}^5 F_i(\mathbf{z}) + \sum_{j=1}^5 g_{i+5} F_i(\mathbf{z}), \quad (16)$$

**Model optimization.** The PBT is optimized by minimizing the mean squared error  $\mathcal{L} = (\hat{y} - y)^2$  using the AdamW<sup>80</sup> optimizer. The hyperparameters that yield the best results for the validation set are selected. The

search ranges of the hyperparameters and selected hyperparameters for pretraining the PBT are listed in Supplementary Table 6.

**PBT specialization.** After pretraining, the resulting model serves as a general PBT that encodes battery lifetime knowledge learned from heterogeneous pretraining datasets. For each target dataset, the general PBT is specialized using the available target-scenario training data. Two transfer learning strategies are considered: fine-tuning, where pretrained model parameters are updated, and adapter tuning, where lightweight trainable modules are inserted while the main pretrained backbone is kept fixed. For fair comparison, the same specialization strategies are applied to CPMLP and CPTransformer. For each model and target dataset, the strategy that achieves the best validation performance is used for testing. Additional implementation details are provided in Supplementary Note 3.

**Evaluation metric.** The MAPE is employed to evaluate model performance and is computed as follows:

$$\text{MAPE} = \frac{|y - \hat{y}|}{y}. \quad (17)$$

### Data availability

All the datasets used in the present study are publicly available, including CALCE<sup>60,64</sup>, MATR<sup>15,16</sup>, RWTH<sup>62</sup>, HUST<sup>20</sup>, Tongji<sup>58</sup>, Stanford<sup>51</sup>, XJTU<sup>59</sup>, and ISU-ILCC<sup>52</sup>. HNEI<sup>56</sup>, SNL<sup>55</sup>, MICH\_EXP<sup>53</sup>, MICH<sup>25</sup>, and UL-PUR<sup>54,61</sup> are hosted in the BatteryArchive (<https://www.batteryarchive.org/>). The Zn-ion, Na-ion and industrial LIB datasets are provided by BatteryLife<sup>13</sup> (<https://github.com/Ruifeng-Tan/BatteryLife>).

### Code availability

The code for the modeling work and data preprocessing is available at <https://github.com/Ruifeng-Tan/PBT>. The weights of the pretrained PBT are available at <https://zenodo.org/records/17972780>.

### Author contributions

T.-Y. Zhang, J. Huang, R. Tan and J. Li conceived the study. R. Tan designed the model and conducted the AI analysis with the help of X. Hong and J. Li. R. Tan, J. Huang and T.-Y. Zhang wrote the paper, with contributions from all the authors. T.-Y. Zhang and J. Huang managed the project and guided the research.

### Acknowledgments

The authors acknowledge financial support from the National Key R&D Program of China (No. 2023YFB2503600). This work is also supported by research grants from the National Natural Science Foundation of China (Nos. 92372109 and 52207230) and the Guangdong Provincial Talent Program (No.2024TQ08X366). We also acknowledge support from the Wilson Tang Brilliant Energy Science and Technology Lab (BEST Lab) at Hong Kong University of Science and Technology (Guangzhou).

### Declaration of interests

The authors declare a competing interest: a Chinese patent application related to the method reported in this work has been filed under application number 202610578824X.

### References

- 1 Huang, J., Boles, S. T. & Tarascon, J.-M. Sensing as the key to battery lifetime and sustainability. *Nature Sustainability* **5**, 194-204 (2022). <https://doi.org/10.1038/s41893-022-00859-y>

- 2 Tao, S. *et al.* Collaborative and privacy-preserving retired battery sorting for profitable direct recycling via federated machine learning. *Nature Communications* **14**, 8032 (2023). <https://doi.org/10.1038/s41467-023-43883-y>
- 3 Liu, H. *et al.* Multi-modal framework for battery state of health evaluation using open-source electric vehicle data. *Nature Communications* **16**, 1137 (2025). <https://doi.org/10.1038/s41467-025-56485-7>
- 4 Figgenger, J. *et al.* Multi-year field measurements of home storage systems and their use in capacity estimation. *Nature Energy* **9**, 1438-1447 (2024). <https://doi.org/10.1038/s41560-024-01620-9>
- 5 Tan, R. *et al.* Forecasting battery degradation trajectory under domain shift with domain generalization. *Energy Storage Materials* **72**, 103725 (2024). <https://doi.org/10.1016/j.ensm.2024.103725>
- 6 Miao, Y., Liu, L., Zhang, Y., Tan, Q. & Li, J. An overview of global power lithium-ion batteries and associated critical metal recycling. *Journal of Hazardous Materials* **425**, 127900 (2022). <https://doi.org/https://doi.org/10.1016/j.jhazmat.2021.127900>
- 7 Fleischmann, J. *et al.* Battery 2030: Resilient, sustainable, and circular. *McKinsey & Company* **16**, 2023 (2023).
- 8 Zheng, H. *et al.* Self-discharge estimation for lithium-ion batteries based on formation data in production. *Engineering Applications of Artificial Intelligence* **169**, 114180 (2026). <https://doi.org/https://doi.org/10.1016/j.engappai.2026.114180>
- 9 Zhang, N. *et al.* Rechargeable aqueous zinc-manganese dioxide batteries with high energy and power densities. *Nature Communications* **8**, 405 (2017). <https://doi.org/10.1038/s41467-017-00467-x>
- 10 Mi, J. *et al.* A ductile solid electrolyte interphase for solid-state batteries. *Nature* **647**, 86-92 (2025). <https://doi.org/10.1038/s41586-025-09675-8>
- 11 Ruan, J. *et al.* Current collector interphase design for high-energy and stable anode-less sodium batteries. *Nature Sustainability* **8**, 530-541 (2025). <https://doi.org/10.1038/s41893-025-01545-5>
- 12 Zhang, H. *et al.* Battery lifetime prediction across diverse ageing conditions with inter-cell deep learning. *Nature Machine Intelligence* (2025). <https://doi.org/10.1038/s42256-024-00972-x>
- 13 Tan, R. *et al.* in *Proceedings of the 31st ACM SIGKDD Conference on Knowledge Discovery and Data Mining V.2* 5789–5800 (Association for Computing Machinery, Toronto ON, Canada, 2025).
- 14 Li, W., Zhang, H., van Vlijmen, B., Dechent, P. & Sauer, D. U. Forecasting battery capacity and power degradation with multi-task learning. *Energy Storage Materials* **53**, 453-466 (2022). <https://doi.org/10.1016/j.ensm.2022.09.013>
- 15 Attia, P. M. *et al.* Closed-loop optimization of fast-charging protocols for batteries with machine learning. *Nature* **578**, 397-402 (2020). <https://doi.org/10.1038/s41586-020-1994-5>
- 16 Severson, K. A. *et al.* Data-driven prediction of battery cycle life before capacity degradation. *Nature Energy* **4**, 383-391 (2019). <https://doi.org/10.1038/s41560-019-0356-8>
- 17 Zhang, T., Tan, R., Zhu, P., Zhang, T.-Y. & Huang, J. Unlocking Ultrafast Diagnosis of Retired Batteries via Interpretable Machine Learning and Optical Fiber Sensors. *ACS Energy Letters* **10**, 862-871 (2025). <https://doi.org/10.1021/acsenergylett.4c03054>
- 18 Tao, S. *et al.* Immediate remaining capacity estimation of heterogeneous second-life lithium-ion batteries via deep generative transfer learning. *Energy & Environmental Science* **18**, 7413-7426 (2025). <https://doi.org/10.1039/d5ee02217g>
- 19 Tao, S. *et al.* Generative learning assisted state-of-health estimation for sustainable battery recycling with random retirement conditions. *Nature Communications* **15**, 10154 (2024). <https://doi.org/10.1038/s41467-024-54454-0>
- 20 Ma, G. *et al.* Real-time personalized health status prediction of lithium-ion batteries using deep transfer learning. *Energy and Environmental Science* **15**, 4083-4094 (2022). <https://doi.org/10.1039/d2ee01676a>
- 21 Zhang, H. *et al.* in *12th International Conference on Learning Representations, ICLR 2024, May 7, 2024 - May 11, 2024*. (International Conference on Learning Representations, ICLR).
- 22 Rhyu, J. *et al.* Systematic feature design for cycle life prediction of lithium-ion batteries during formation. *Joule*, 101884 (2025). <https://doi.org/10.1016/j.joule.2025.101884>

- 23 Kim, M., Kim, I., Kim, J. & Choi, J. W. Lifetime Prediction of Lithium Ion Batteries by Using the Heterogeneity of Graphite Anodes. *ACS Energy Letters* **8**, 2946-2953 (2023). <https://doi.org/10.1021/acseenergylett.3c00695>
- 24 Sugiarto, L., Huang, Z. & Lu, Y.-C. Battery lifetime prediction using surface temperature features from early cycle data. *Energy & Environmental Science* **18**, 2511-2523 (2025). <https://doi.org/10.1039/d4ee05179c>
- 25 Weng, A. *et al.* Predicting the impact of formation protocols on battery lifetime immediately after manufacturing. *Joule* **5**, 2971-2992 (2021). <https://doi.org/10.1016/j.joule.2021.09.015>
- 26 Geslin, A. *et al.* Selecting the appropriate features in battery lifetime predictions. *Joule* **7**, 1956-1965 (2023). <https://doi.org/10.1016/j.joule.2023.07.021>
- 27 Tao, S. *et al.* Battery Cross-Operation-Condition Lifetime Prediction via Interpretable Feature Engineering Assisted Adaptive Machine Learning. *ACS Energy Letters* **8**, 3269-3279 (2023). <https://doi.org/10.1021/acseenergylett.3c01012>
- 28 Guo, N. *et al.* Semi-supervised learning for explainable few-shot battery lifetime prediction. *Joule* **8**, 1820-1836 (2024). <https://doi.org/10.1016/j.joule.2024.02.020>
- 29 Zhang, J. *et al.* Discovery Learning predicts battery cycle life from minimal experiments. *Nature* **650**, 110-115 (2026). <https://doi.org/10.1038/s41586-025-09951-7>
- 30 Guha, A. & Patra, A. Online Estimation of the Electrochemical Impedance Spectrum and Remaining Useful Life of Lithium-Ion Batteries. *IEEE Transactions on Instrumentation and Measurement* **67**, 1836-1849 (2018). <https://doi.org/10.1109/TIM.2018.2809138>
- 31 Fei, Z., Zhang, Z., Yang, F. & Tsui, K.-L. A deep attention-assisted and memory-augmented temporal convolutional network based model for rapid lithium-ion battery remaining useful life predictions with limited data. *Journal of Energy Storage* **62**, 106903 (2023). <https://doi.org/10.1016/j.est.2023.106903>
- 32 Hsu, C.-W., Xiong, R., Chen, N.-Y., Li, J. & Tsou, N.-T. Deep neural network battery life and voltage prediction by using data of one cycle only. *Applied Energy* **306**, 118134 (2022). <https://doi.org/https://doi.org/10.1016/j.apenergy.2021.118134>
- 33 Cha, J. *et al.* in *35th Conference on Neural Information Processing Systems, NeurIPS 2021, December 6, 2021 - December 14, 2021*. 22405-22418 (Neural information processing systems foundation).
- 34 Kokkalis, K., Chronis, C., Politi, E., Dimitrakopoulos, G. & Varlamis, I. in *2024 IEEE 10th International Conference on Big Data Computing Service and Machine Learning Applications (BigDataService)*. 122-129.
- 35 Zhang, Z., Wang, Y., Ruan, X. & Zhang, X. Lithium-ion batteries lifetime early prediction using domain adversarial learning. *Renewable and Sustainable Energy Reviews* **208**, 115035 (2025). <https://doi.org/10.1016/j.rser.2024.115035>
- 36 Liang, Y. *et al.* in *30th ACM SIGKDD Conference on Knowledge Discovery and Data Mining, KDD 2024, August 25, 2024 - August 29, 2024*. 6555-6565 (Association for Computing Machinery).
- 37 Bommasani, R. On the opportunities and risks of foundation models. *arXiv preprint arXiv:2108.07258* (2021).
- 38 Qing, P. *et al.* 20511-20523 (Association for Computational Linguistics).
- 39 Zhao, C. *et al.* Learning Domain Invariant Prompt for Vision-Language Models. *IEEE Trans Image Process* **33**, 1348-1360 (2024). <https://doi.org/10.1109/TIP.2024.3362062>
- 40 Zheng, H. *et al.* Learning from models beyond fine-tuning. *Nature Machine Intelligence* **7**, 6-17 (2025). <https://doi.org/10.1038/s42256-024-00961-0>
- 41 Jiang, J., Zuo, Z., Wu, G., Jiang, K. & Liu, X. A Survey on All-in-One Image Restoration: Taxonomy, Evaluation and Future Trends. *IEEE Transactions on Pattern Analysis and Machine Intelligence* **47**, 11892-11911 (2025). <https://doi.org/10.1109/TPAMI.2025.3598132>
- 42 Zeng, F., Zhu, F., Guo, H., Zhang, X.-Y. & Liu, C.-L. 12137-12152 (Association for Computational Linguistics).
- 43 Guo, D. *et al.* DeepSeek-R1 incentivizes reasoning in LLMs through reinforcement learning. *Nature* **645**, 633-638 (2025). <https://doi.org/10.1038/s41586-025-09422-z>

- 44 Dai, D. *et al.* in *62nd Annual Meeting of the Association for Computational Linguistics, ACL 2024, August 11, 2024 - August 16, 2024*. 1280-1297 (Association for Computational Linguistics (ACL)).
- 45 Achiam, J. *et al.* Gpt-4 technical report. *arXiv preprint arXiv:2303.08774* (2023).
- 46 Brown, T. B. *et al.* in *34th Conference on Neural Information Processing Systems, NeurIPS 2020, December 6, 2020 - December 12, 2020*. Apple; et al.; Microsoft; PDT Partners; Sony; Tenstorrent (Neural information processing systems foundation).
- 47 Redmon, J., Divvala, S., Girshick, R. & Farhadi, A. in *29th IEEE Conference on Computer Vision and Pattern Recognition, CVPR 2016, June 26, 2016 - July 1, 2016*. 779-788 (IEEE Computer Society).
- 48 Dosovitskiy, A. *et al.* in *9th International Conference on Learning Representations, ICLR 2021, May 3, 2021 - May 7, 2021*. Amazon; DeepMind; et al.; Facebook AI; Microsoft; OpenAI (International Conference on Learning Representations, ICLR).
- 49 Radford, A. *et al.* in *38th International Conference on Machine Learning, ICML 2021, July 18, 2021 - July 24, 2021*. 8748-8763 (ML Research Press).
- 50 He, K., Zhang, X., Ren, S. & Sun, J. in *29th IEEE Conference on Computer Vision and Pattern Recognition, CVPR 2016, June 26, 2016 - July 1, 2016*. 770-778 (IEEE Computer Society).
- 51 Cui, X. *et al.* Data-driven analysis of battery formation reveals the role of electrode utilization in extending cycle life. *Joule* **8**, 3072-3087 (2024). <https://doi.org/https://doi.org/10.1016/j.joule.2024.07.024>
- 52 Li, T., Zhou, Z., Thelen, A., Howey, D. A. & Hu, C. Predicting battery lifetime under varying usage conditions from early aging data. *Cell Reports Physical Science* **5**, 101891 (2024). <https://doi.org/10.1016/j.xcrp.2024.101891>
- 53 Mohtat, P., Lee, S., Siegel, J. B. & Stefanopoulou, A. G. Reversible and Irreversible Expansion of Lithium-Ion Batteries Under a Wide Range of Stress Factors. *Journal of The Electrochemical Society* **168**, 100520 (2021). <https://doi.org/10.1149/1945-7111/ac2d3e>
- 54 Juarez-Robles, D., Jeevarajan, J. A. & Mukherjee, P. P. Degradation-Safety Analytics in Lithium-Ion Cells: Part I. Aging under Charge/Discharge Cycling. *Journal of The Electrochemical Society* **167**, 160510 (2020). <https://doi.org/10.1149/1945-7111/abc8c0>
- 55 Preger, Y. *et al.* Degradation of Commercial Lithium-Ion Cells as a Function of Chemistry and Cycling Conditions. *Journal of The Electrochemical Society* **167**, 120532 (2020). <https://doi.org/10.1149/1945-7111/abae37>
- 56 Devie, A., Baure, G. & Dubarry, M. Intrinsic Variability in the Degradation of a Batch of Commercial 18650 Lithium-Ion Cells. *Energies* **11**, 1031 (2018).
- 57 Lin, M. *et al.* Lithium-ion battery degradation trajectory early prediction with synthetic dataset and deep learning. *Journal of Energy Chemistry* **85**, 534-546 (2023). <https://doi.org/https://doi.org/10.1016/j.jechem.2023.06.036>
- 58 Zhu, J. *et al.* Data-driven capacity estimation of commercial lithium-ion batteries from voltage relaxation. *Nature Communications* **13**, 2261 (2022). <https://doi.org/10.1038/s41467-022-29837-w>
- 59 Wang, F., Zhai, Z., Zhao, Z., Di, Y. & Chen, X. Physics-informed neural network for lithium-ion battery degradation stable modeling and prognosis. *Nature Communications* **15**, 4332 (2024). <https://doi.org/10.1038/s41467-024-48779-z>
- 60 Xing, Y., Ma, E. W. M., Tsui, K.-L. & Pecht, M. An ensemble model for predicting the remaining useful performance of lithium-ion batteries. *Microelectronics Reliability* **53**, 811-820 (2013). <https://doi.org/https://doi.org/10.1016/j.microrel.2012.12.003>
- 61 Juarez-Robles, D., Azam, S., Jeevarajan, J. A. & Mukherjee, P. P. Degradation-Safety Analytics in Lithium-Ion Cells and Modules: Part III. Aging and Safety of Pouch Format Cells. *Journal of The Electrochemical Society* **168**, 110501 (2021). <https://doi.org/10.1149/1945-7111/ac30af>
- 62 Li, W. *et al.* One-shot battery degradation trajectory prediction with deep learning. *Journal of Power Sources* **506**, 230024 (2021). <https://doi.org/10.1016/j.jpowsour.2021.230024>
- 63 Huang, X. *et al.* Physics-informed mixture of experts network for interpretable battery degradation trajectory computation amid second-life complexities. *arXiv preprint arXiv:2506.17755* (2025).

- 64 He, W., Williard, N., Osterman, M. & Pecht, M. Prognostics of lithium-ion batteries based on Dempster–Shafer theory and the Bayesian Monte Carlo method. *Journal of Power Sources* **196**, 10314-10321 (2011). <https://doi.org/10.1016/j.jpowsour.2011.08.040>
- 65 Cai, W. *et al.* A Survey on Mixture of Experts in Large Language Models. *IEEE Transactions on Knowledge and Data Engineering*, 1-20 (2025). <https://doi.org/10.1109/tkde.2025.3554028>
- 66 Li, Q. *et al.* The critical importance of stack pressure in batteries. *Nature Energy* (2025). <https://doi.org/10.1038/s41560-025-01820-x>
- 67 Liu, C. *et al.* Air-stable Li<sub>5</sub>FeO<sub>4</sub> additive enabled by carbon coating for energy-dense lithium-ion batteries. *Nature Communications* **16**, 7694 (2025). <https://doi.org/10.1038/s41467-025-62418-1>
- 68 Guo, J. *et al.* Degradation and Failure Mechanisms of Lithium/LiNixCoyMn1-x-yO<sub>2</sub> Batteries. *ACS Energy Letters* **10**, 2318-2340 (2025). <https://doi.org/10.1021/acseenergylett.4c03578>
- 69 Birkl, C. R., Roberts, M. R., McTurk, E., Bruce, P. G. & Howey, D. A. Degradation diagnostics for lithium ion cells. *Journal of Power Sources* **341**, 373-386 (2017). <https://doi.org/10.1016/j.jpowsour.2016.12.011>
- 70 Schimpe, M. *et al.* Comprehensive Modeling of Temperature-Dependent Degradation Mechanisms in Lithium Iron Phosphate Batteries. *Journal of The Electrochemical Society* **165**, A181 (2018). <https://doi.org/10.1149/2.1181714jes>
- 71 Waldmann, T., Wilka, M., Kasper, M., Fleischhammer, M. & Wohlfahrt-Mehrens, M. Temperature dependent ageing mechanisms in Lithium-ion batteries - A Post-Mortem study. *Journal of Power Sources* **262**, 129-135 (2014). <https://doi.org/10.1016/j.jpowsour.2014.03.112>
- 72 Liu, Y. *et al.* in *12th International Conference on Learning Representations, ICLR 2024, May 7, 2024 - May 11, 2024*. (International Conference on Learning Representations, ICLR).
- 73 Nie, Y., Nguyen, N. H., Sinthong, P. & Kalagnanam, J. in *11th International Conference on Learning Representations, ICLR 2023, May 1, 2023 - May 5, 2023*. Baidu; DeepMind; et al.; Google Research; Huawei; Meta AI (International Conference on Learning Representations, ICLR).
- 74 Wang, H. *et al.* in *11th International Conference on Learning Representations, ICLR 2023, May 1, 2023 - May 5, 2023*. Baidu; DeepMind; et al.; Google Research; Huawei; Meta AI (International Conference on Learning Representations, ICLR).
- 75 Zeng, A., Chen, M., Zhang, L. & Xu, Q. in *37th AAAI Conference on Artificial Intelligence, AAAI 2023, February 7, 2023 - February 14, 2023*. 11121-11128 (AAAI Press).
- 76 Grattafiori, A. *et al.* The llama 3 herd of models. *arXiv preprint arXiv:2407.21783* (2024).
- 77 Ba, J. L. Layer normalization. *arXiv preprint arXiv:1607.06450* (2016).
- 78 Hendrycks, D. Gaussian Error Linear Units (Gelu). *arXiv preprint arXiv:1606.08415* (2016).
- 79 Vaswani, A. *et al.* in *31st Annual Conference on Neural Information Processing Systems, NIPS 2017, December 4, 2017 - December 9, 2017*. 5999-6009 (Neural information processing systems foundation).
- 80 Loshchilov, I. & Hutter, F. in *7th International Conference on Learning Representations, ICLR 2019, May 6, 2019 - May 9, 2019*. (International Conference on Learning Representations, ICLR).

# Supplementary Information

## **Pretrained battery transformer (PBT): A foundation model for battery life prediction**

Ruifeng Tan<sup>1,2</sup>, Weixiang Hong<sup>1</sup>, Jia Li<sup>3\*</sup>, Jiaqiang Huang<sup>1,4,5\*</sup> and Tong-Yi Zhang<sup>6\*</sup>

<sup>1</sup>Guangzhou Municipal Key Laboratory of Materials Informatics and Sustainable Energy and Environment Thrust, The Hong Kong University of Science and Technology (Guangzhou), Nansha, Guangzhou, 511400, Guangdong, P. R. China.

<sup>2</sup>Department of Computer Science & Engineering, The Hong Kong University of Science and Technology, Clear Water Bay, Kowloon, 999077, Hong Kong, P. R. China.

<sup>3</sup>Guangzhou Municipal Key Laboratory of Materials Informatics and Data Science and Analytics Thrust, The Hong Kong University of Science and Technology (Guangzhou), Nansha, Guangzhou, 511400, Guangdong, P. R. China.

<sup>4</sup>Academy of Interdisciplinary Studies, The Hong Kong University of Science and Technology, Clear Water Bay, Kowloon, 999077, Hong Kong, P. R. China.

<sup>5</sup>Guangzhou HKUST Fok Ying Tung Research Institute, Nansha District, Guangzhou, 511458, Guangdong, P. R. China.

<sup>6</sup>Material Genome Institute, Shanghai University, 333 Nanchen Road, Shanghai 200444, P. R. China; Guangzhou Municipal Key Laboratory of Materials Informatics, Advanced Materials Thrust, and Sustainable Energy and Environment Thrust, The Hong Kong University of Science and Technology (Guangzhou), Nansha, Guangzhou, 511400, Guangdong, P. R. China.

\*Corresponding authors.

E-mails: [jjalee@ust.hk](mailto:jjalee@ust.hk); [seejhuang@hkust-gz.edu.cn](mailto:seejhuang@hkust-gz.edu.cn); [mezhangt@hkust-gz.edu.cn](mailto:mezhangt@hkust-gz.edu.cn)

## Supplementary Notes

### Supplementary Note 1. Details of data preprocessing

We first preprocess all datasets used in this study using the data preprocessing scripts provided in BatteryLife<sup>1</sup>. We then exclude batteries with a cycle life shorter than 100 cycles, as such lifetimes are shorter than the input window used for prediction. Following BatteryLife, we also remove batteries whose state of health (SOH) does not decline to  $\lambda + 2.5\%$ . Here,  $\lambda$  is set 90% for the industrial lithium-ion dataset, because most batteries in this dataset do not degrade to 80%, and to 80% for all other datasets. For batteries whose SOH declines to  $\lambda + 2.5\%$  but not to  $\lambda$ , we estimate cycle life by linear extrapolation.

### Supplementary Note 2. Details of ageing conditions of the five batteries shown in Fig. 1c

The file names (the names are sourced from the raw files) and ageing conditions as well as cycle life of the five batteries shown in Fig. 1c are as follows:

1. **HNEI\_18650\_NMC\_LCO\_25C\_0-100\_0.5-1.5C\_e**: The cycle life is 259. This is a lithium-ion battery (LIB) in a format of 18650 cylindrical battery. Its positive electrode is a mixture of  $\text{LiCoO}_2$  (LCO) and  $\text{LiNi}_{0.4}\text{Co}_{0.4}\text{Mn}_{0.2}\text{O}_2$  (NCM442). Its negative electrode is graphite. The electrolyte formula is unknown. The battery manufacturer is LG Chemical Limited. The working ambient temperature of this battery is 25 degrees Celsius. The cycling consists of three different strategies. For 1<sup>st</sup> to 10<sup>th</sup> cycles, the battery was charged at a constant current of 0.5 C until reaching 4.3 V, then was discharged at a constant current of 0.5 C until reaching 3 V. The cycling state-of-charge of this battery ranges from 0% to 100%.
2. **MICH\_05C\_pouch\_NMC\_-5C\_0-100\_1.5-1.5C**: The cycle life is 325. This is a LIB in a format of pouch battery. Its positive electrode is  $\text{Li}(\text{Ni}_{0.33}\text{Co}_{0.33}\text{Mn}_{0.33})\text{O}_2$  (NCM111). Its negative electrode is graphite. The electrolyte formula consists of 1M  $\text{LiPF}_6$  salt in solvents of ethylene carbonate (EC) and ethyl methyl carbonate (EMC) with a ratio of 3:7. The battery manufacturer is LISHEN. The nominal capacity is 5.0 Ah. The working ambient temperature of this battery is -5 degrees Celsius. In the cycling, the battery was charged at a constant current of 1.5 C until reaching 4.2 V, and then 4.2 V was sustained until the current dropped to 0.02 C. The battery was then discharged at a constant current of 1.5 C until reaching 3.0 V. The cycling state-of-charge of this battery ranges from 0% to 100%.
3. **XJTU\_2C\_battery-8**: The cycle life is 420. This is a LIB in a format of 18650 cylindrical battery. Its positive electrode is  $\text{Li}(\text{Ni}_{0.5}\text{Co}_{0.2}\text{Mn}_{0.3})\text{O}_2$  (NCM523). Its negative electrode is graphite. The electrolyte formula is unknown. The battery manufacturer is LISHEN. The nominal capacity is 2 Ah. The working ambient

temperature of this battery is 20 degrees Celsius. In the cycling, the battery was charged at a constant current of 2 C until reaching 4.2 V, and then 4.2 V was sustained until the current dropped to 0.05 C. And then rest for 5 minutes. The battery was then discharged at a constant current of 1 C until reaching 2.5 V, and then rest for 5 minutes. The cycling state-of-charge of this battery ranges from 0% to 100%.

4. **RWTH\_010, MATR\_b1c2:** The cycle life is 696. This is a LIB in a format of 18650 cylindrical battery. Its positive electrode is NCM and negative electrode is carbon. The electrolyte formula is unknown. The battery manufacturer is Sanyo/Panasonic. The nominal capacity is 3 Ah. The working ambient temperature of this battery is 25 degrees Celsius. In the cycling, the battery was discharged at a constant current of 2 C until reaching 3.5 V. The battery was then charged at a constant current of 2 C until reaching 3.9 V. The cycling state-of-charge of this battery ranges from 20% to 80%.
5. **MATR\_b1c2:** The cycle life is 2237. This is a LIB in a format of 18650 cylindrical battery. Its positive electrode is a lithium iron phosphate ( $\text{LiFePO}_4$ ). Its negative electrode is graphite. The electrolyte formula is unknown. The battery manufacturer is A123 system. The nominal capacity is 1.1 Ah. Operating condition: The working history of this battery is just after formation. The working ambient temperature of this battery is 30 degrees Celsius. In the cycling, the battery was charged at a constant current of 3.6 C to 80% state-of-charge (SOC) until reaching 3.6 V. The battery was then discharged at a constant current of 4 C until reaching 2 V. The cycling state-of-charge of this battery ranges from 0% to 100%.

### Supplementary Note 3. Implementation details of transfer learning methods

In this work, we utilized two kinds of transfer learning methods: fine-tuning and adapter tuning<sup>2</sup>. For fine-tuning, all parameters of the pretrained model are updated using (i) a learning rate selected from  $10^{-5}$  to  $10^{-4}$ , (ii) a batch size chosen from [4,8,16,32,64,128,256], (iii) a weight decay in the AdamW<sup>3</sup> optimizer selected from [0,10.0], and (iv) a dropout rate from [0.0,0.05,0.15,0.25].

For adapter tuning, we insert adapter layers after the first  $N$  layers of the pretrained model. Each adapter transforms the input as:

$$\hat{x} = W_2 \text{GELU}(W_1 \text{LN}(x) + b_1) + b_2, \quad (1)$$

where  $x \in \mathbb{R}^d$ ,  $W_1 \in \mathbb{R}^{d \times d_a}$  and  $b_1 \in \mathbb{R}^{d_a}$  are learnable parameters,  $W_2 \in \mathbb{R}^{d_a \times d}$  and  $b_2 \in \mathbb{R}^d$  are learnable parameters,  $\text{LN}(\cdot)$  denotes the layer normalization<sup>4</sup>, and  $d_a$  denotes the adapter embedding dimension. We tune  $N$  from [1,12] (PBT contains 12 encoder layers), batch size from [4,8,16,32,64,128,256], learning rate

from  $[5 \times 10^{-6}, 10^{-3}]$ , weight decay from  $[0, 10.0]$ , dropout rate from  $[0.0, 0.05, 0.15, 0.25]$ , and  $d_a$  from  $[1, 128]$ . Final hyperparameters for both transfer learning methods are selected based on validation performance.

#### Supplementary Note 4. Implementation details of BatLiNet

The BatLiNet is reproduced using the official code available at <https://codeocean.com/capsule/2426768/tree/v2>.

We used the same dataset splits of the present study for training BatLiNet and tuned the hyperparameters of it to facilitate fair comparisons. For the hyperparameters, we selected a dropout from  $[0, 0.5]$ , and a batch size chosen from  $[32, 64, 128]$ . Additionally, we tune two hyperparameters as follows:

1. `diff_base`: Let  $x_i$  denotes the features of the  $i^{th}$  cycle. BatLiNet computes  $x_i - x_{diff\_base}$  as the features of  $i^{th}$  cycle. We selected `diff_base` from  $[10, 15, 20]$ .
2.  $\alpha$ : BatLiNet relies on an intra-cell learning branch and inter-cell learning branch, and alpha is a hyperparameter used to balance the loss and prediction from the two branches:  $\mathcal{L} = \alpha \mathcal{L}_{intra} + (1 - \alpha) \mathcal{L}_{inter}$  and  $\hat{y} = \alpha \hat{y}_{intra} + (1 - \alpha) \hat{y}_{inter}$ . We selected  $\alpha$  from  $[0, 0.2, 0.5, 0.8]$ .

To specify the reference batteries (source domains) for transfer learning in BatLiNet, two configurations were considered:

1. LiFePO<sub>4</sub> source domain (aligned with the original implementation): Reference batteries were randomly sampled from LiFePO<sub>4</sub> cells in the MATR, HUST, and SNL datasets.
2. Broader and more heterogeneous corpus: Reference batteries were randomly sampled from 13 datasets (CALCE, HNEI, MATR, SNL, UL\_PUR, MICH\_EXP, MICH, HUST, Tongji, Stanford, ISU\_ILCC, and XJTU datasets), covering diverse ageing conditions.

All experiments were executed three times with distinct random seeds. Performance is reported as mean  $\pm$  standard deviation and is summarized in Supplementary Table 3 and Supplementary Table 4. We note that BatLiNet relies on a fixed number of collected cycles for lifetime prediction. Given the substantial computational overhead of BatLiNet (validation on 15 datasets costed two months using 16 RTX 4090 GPUs), we restricted our evaluation to the version utilizing the first 20 cycles as input. For the BatLiNet configuration using the 13 datasets as source domains, we reproduced its performance on only 9 downstream datasets because of the time-intensive training procedure.

### Supplementary Note 5. Further details of BatteryMoE-CyclePatch

Given the voltage and current time series, we compute the capacity for a given charging/discharging period using the Coulomb counting method:

$$Q = \int_{t_1}^{t_2} |I| dt, \quad (2)$$

where  $t_1$  is the start time of charging/discharging, and  $t_2$  is any time within the same charging/discharging period. This procedure provides the corresponding capacity values. Because different cycles contain different numbers of sampled points, we resample each cycle to 300 data points, with 150 points for charging and 150 points for discharging. Each point includes voltage, current, and capacity records. For consistency across datasets, voltage is expressed in volts, current in C-rate, and capacity in ampere-hours (Ah).

## Supplementary Tables

**Supplementary Table 1.** The statistics of each dataset that is included in the present study. The statistics are conducted on the processed datasets.

<b>Dataset</b>	<b>Battery number</b>	<b>Formats</b>	<b>Chemical Systems</b>	<b>Operating Temperatures</b>	<b>Protocols</b>	<b>Aging conditions</b>
CALCE	13	1	1	1	2	4
HNEI	14	1	1	1	2	2
MATR	169	1	1	1	81	81
UL_PUR	2	1	1	1	1	1
SNL	50	1	3	3	5	19
MICH_EXP	8	1	1	3	6	8
MICH	40	1	1	2	2	4
RWTH	48	1	1	1	1	1
HUST	77	1	1	1	77	77
Tongji	99	1	3	3	5	10
Stanford	38	1	1	1	1	14
XJTU	23	1	1	1	2	2
ISU_ILCC	239	1	1	1	195	195
Zn-ion	99	3	45	3	1	99
Na-ion	31	1	1	1	12	12
Industrial Li-ion	27	1	1	4	2	4
Total	977	8	61	9	395	528

**Supplementary Table 2.** The chemistries of the collected 16 datasets in this study.

Dataset	Positive electrode	Negative electrode	Electrolyte
CALCE	LiCoO <sub>2</sub> (LCO)	Graphite	Unknown
MATR	LiFePO <sub>4</sub> (LFP)	Graphite	Unknown
HUST	LFP	Graphite	Unknown
HNEI	LCO/ (NCM442)	LiNi <sub>0.4</sub> Co <sub>0.4</sub> Mn <sub>0.2</sub> O <sub>2</sub> Graphite	Unknown
RWTH	NCM	Carbon	Unknown
SNL	LFP/ LiNi <sub>0.81</sub> Co <sub>0.14</sub> Al <sub>0.05</sub> O <sub>2</sub> (NCA811405)/ LiNi <sub>0.84</sub> Co <sub>0.1</sub> Mn <sub>0.06</sub> O <sub>2</sub> (NCM840610)	Graphite	Unknown
UL-PUR	NCA801505	Graphite	Unknown
MICH	NCM111	Graphite	1.0 M LiPF <sub>6</sub> Salt, EC:EMC(3:7) and 2wt% VC
MICH-EXP	NCM111	Graphite:PVDF (95:5)	1 M LiPF <sub>6</sub> with 2% EC:EMC (3:7)
Stanford	NCM523	Artificial Graphite	1 M LiPF <sub>6</sub> in EC/EMC/DMC (1 : 1 : 1 by volume) solvent with 2% VC (by weight) additive
Tongji	NCA861103/ NCM831107 /42 wt.% LiNiCoMnO <sub>2</sub> blended with 58 wt.% LiNiCoAlO <sub>2</sub>	Graphite/ wt.% Si Graphite	2 non-aqueous + solution with LiPF <sub>6</sub>
XJTU	NCM523	Graphite	Unknown
ISU-ILCC	NCM	Graphite	Unknown
Zn-ion	MnO <sub>2</sub>	Zinc	2 M ZnSO <sub>4</sub> in H <sub>2</sub> O with multiple additives
Na-ion	Unknown	Unknown	Unknown
CALB	NCM	Graphite	Unknown

**Supplementary Table 3.** The comparison between PBT and BatLiNet<sup>5</sup> on testing sets of the collected 15 datasets. The “Imp” denotes the relative improvement of PBT-TL over BatLiNet. Both models have only the first 20 cycles as the input.

Dataset	PBT-TL	BatLiNet	Imp	Training battery number
HNEI	<b>0.033±0.002</b>	1.419±0.136	97.65%	9
MATR	<b>0.077±0.006</b>	0.161±0.031	51.85%	102
MICH	<b>0.084±0.007</b>	0.353±0.050	76.01%	24
XJTU	<b>0.055±0.010</b>	1.408±0.107	96.04%	15
Stanford	<b>0.094±0.012</b>	0.104±0.008	9.26%	25
RWTH	<b>0.082±0.003</b>	0.175±0.135	53.14%	30
MICH_EXP	<b>0.061±0.035</b>	1.16±0.175	94.71%	7
Tongji	<b>0.134±0.002</b>	0.195±0.018	31.39%	66
HUST	<b>0.098±0.014</b>	0.121±0.003	18.95%	47
SNL	<b>0.143±0.006</b>	1.836±0.428	92.17%	30
ISU_ILCC	<b>0.210±0.007</b>	0.857±0.054	75.41%	144
CALCE	<b>0.191±0.056</b>	1.22±0.712	84.39%	9
Industrial Li-ion	<b>0.097±0.029</b>	3.667±2.863	97.35%	17
Na-ion	<b>0.237±0.004</b>	1.85±0.243	87.16%	20
Zn-ion	<b>0.396±0.056</b>	1.617±0.192	75.51%	60

**Supplementary Table 4.** The comparison between PBT and BatLiNet<sup>5</sup> on testing sets of the collected 15 datasets. In this table, the BatLiNet-Large uses the pretraining data of PBT as the source domains. BatLiNet only uses LFP/graphite cells as source domains. Due to the time-intensive training procedure, we reproduced the performance of BatLiNet-Large on only 9 downstream datasets. The “Imp” denotes the relative improvement of PBT-TL over BatLiNet-Large. Both models have only the first 20 cycles as the input.

Dataset	PBT-TL	BatLiNet-Large	BatLiNet	Imp	Training battery number
HNEI	<b>0.033±0.002</b>	0.046±0.010	1.419±0.136	28.26%	9
MATR	<b>0.077±0.006</b>	-	0.161±0.031	-	102
MICH	<b>0.084±0.007</b>	-	0.353±0.050	-	24
XJTU	<b>0.055±0.010</b>	-	1.408±0.107	-	15
Stanford	<b>0.094±0.012</b>	-	0.104±0.008	-	25
RWTH	<b>0.082±0.003</b>	-	0.175±0.135	-	30
MICH_EXP	<b>0.061±0.035</b>	0.967±0.149	1.16±0.175	93.69%	7
Tongji	<b>0.134±0.002</b>	0.308±0.010	0.195±0.018	56.49%	66
HUST	<b>0.098±0.014</b>	0.129±0.005	0.121±0.003	24.03%	47
SNL	<b>0.143±0.006</b>	-	1.836±0.428	-	30
ISU_ILCC	<b>0.210±0.007</b>	0.481±0.024	0.857±0.054	56.34%	144
CALCE	<b>0.191±0.056</b>	11.163±12.171	1.22±0.712	98.28%	9
Industrial Li-ion	<b>0.097±0.029</b>	1.524±1.052	3.667±2.863	93.6%	17
Na-ion	<b>0.237±0.004</b>	1.645±0.359	1.85±0.243	85.59%	20
Zn-ion	<b>0.396±0.056</b>	1.383±0.200	1.617±0.192	71.3%	60

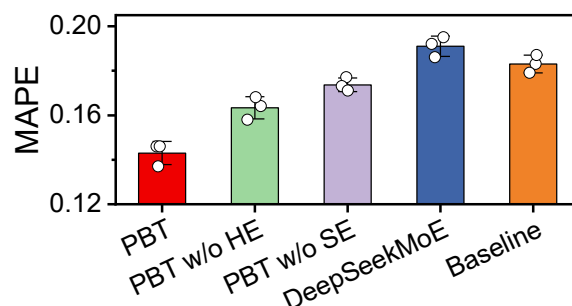
**Supplementary Table 5.** Results of directly applying the pretrained models to industrial Li-ion, Na-ion and Zn-ion datasets. The results are evaluated by MAPE.

Model	Industrial Li-ion	Na-ion	Zn-ion
PBT	1.559±0.205	4.146±1.774	2.516±1.302
CPMLP	1.546±0.045	10.001±0.981	8.333±0.619
CPTransformer	2.030±0.231	10.789±1.065	8.950±0.892

**Supplementary Table 6.** Selected hyperparameters used in model training. The table lists the key hyperparameters and their optimized values used for the Pretrained Battery Transformer (PBT). The notation  $d_{ff}$  and  $d$  follow the definitions in the Methods section.

Hyperparameters	Searching range	Selected value
Learning rate	$10^{-3}$ - $10^{-5}$	$2.5 \times 10^{-5}$
Batch size	128, 256	256
The number of attention heads	4, 8, 16	8
The number of encoder layers	1-12	2
The number of decoder layers	1-12	10
$d_{ff}$ (see Methods)	256, 512	512
Embedding dimension of CyclePatch ( $d$ , see Methods)	32, 64, 128, 256	128
Dropout rate	0.0, 0.05, 0.25	0.05
Embedding dimension of FFN	64, 128, 256	128

## Supplementary Figures



**Supplementary Figure 1. Ablation studies evaluating the efficacy of the proposed hard encoder (HE) and soft encoder (SE).** PBT denotes the proposed Pretrained Battery Transformer. “w/o” denotes the exclusion of a technique; for example, “w/o HE” refers to the removal of hard encoder. DeepSeekMoE<sup>6</sup> is shown as a reference model naively applying a generic language MoE to battery data. Baseline corresponds to the PBT without BatteryMoE.

a

Task description: The target is the number of cycles until the battery’s discharge capacity reaches [x]% of its nominal capacity. The discharge capacity is calculated under the described operating condition. Please directly output the target of the battery based on the provided data.

Battery specifications: The data comes from a [x]-ion battery in a format of [x]. Its positive electrode is [x]. Its negative electrode is [x]. The electrolyte formula is [x]. The battery manufacturer is [x]. The nominal capacity is [x].

Operating condition: [If the formation protocol is available, include it here. Otherwise, indicate that the battery’s operating history begins immediately after formation.]. The working ambient temperature of this battery is [x] degrees Celsius. The cycling consists of [A] charging stages. In the first stage, the battery was charged at a constant current of [x] C to [x]% state-of-charge (SOC). ... In the A<sup>th</sup> stage, the battery was charged at a constant current of [x] C to [x]% SOC. The discharging consists of [B] stages. In the first stage, the battery was discharged at a constant current of [x] C to [x]% SOC. ... In the B<sup>th</sup> stage, the battery was discharged at a constant current of [x] C to [x]% SOC. The cycling state-of-charge of this battery ranges from [x]% to [x].

Note: If there is only one charging/discharging stage, we will directly describe the single charging/discharging stage.

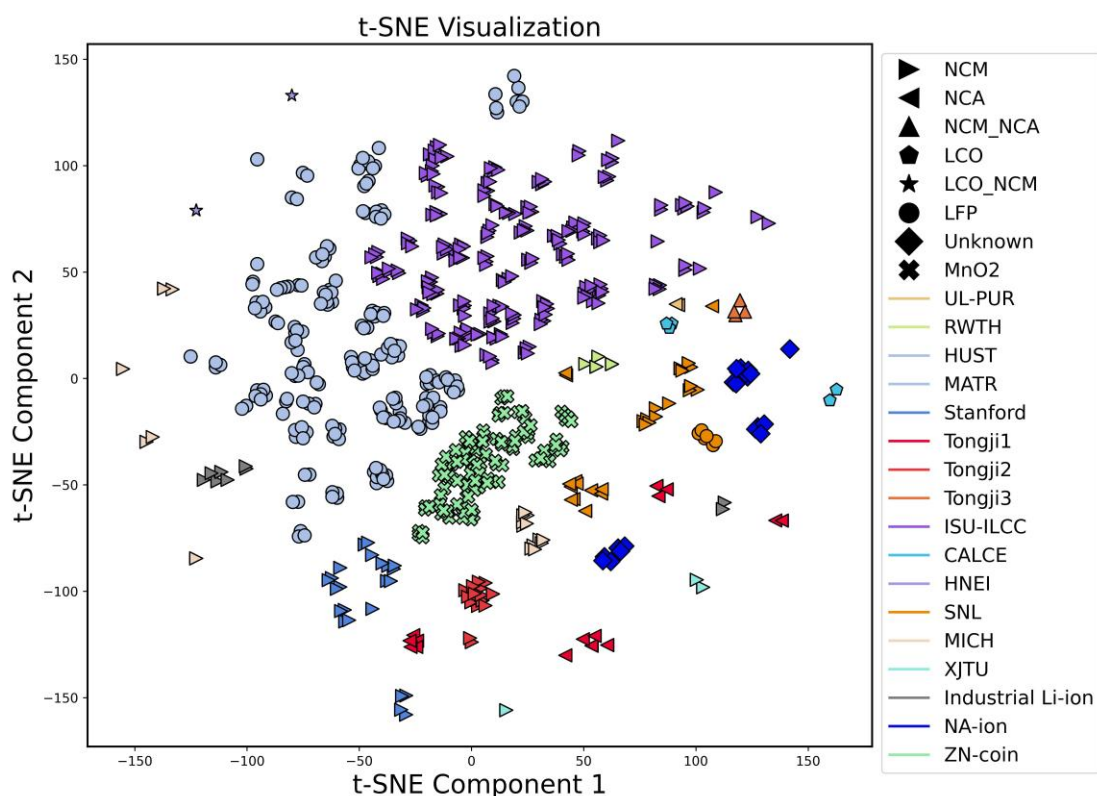
b

Task description: The target is the number of cycles until the battery’s discharge capacity reaches 80% of its nominal capacity. The discharge capacity is calculated under the described operating condition. Please directly output the target of the battery based on the provided data.

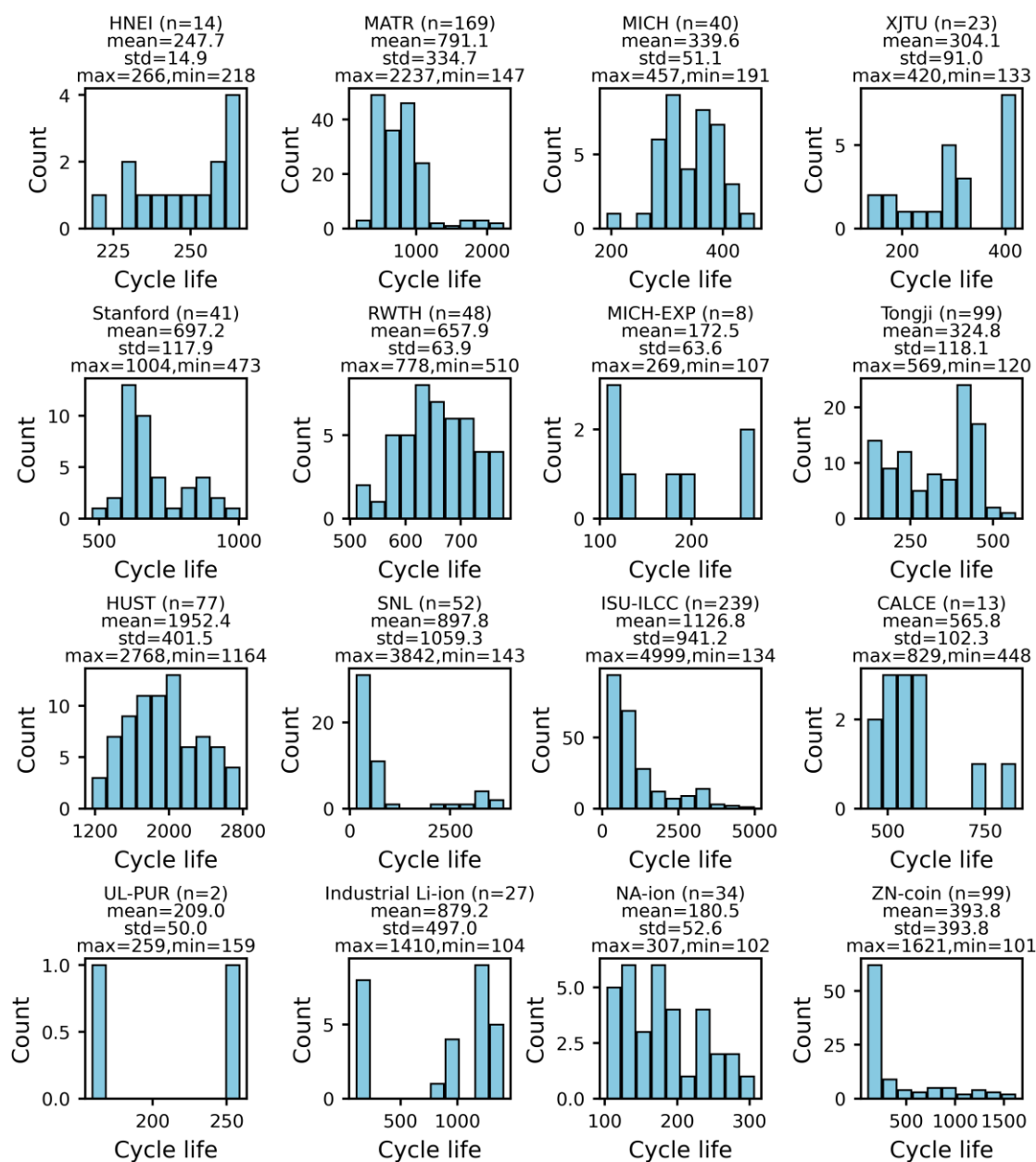
Battery specifications: The data comes from a lithium-ion battery in a format of 18650 cylindrical battery. Its positive electrode is a lithium iron phosphate (LiFePO<sub>4</sub>). Its negative electrode is graphite. The electrolyte formula is unknown. The battery manufacturer is A123 system. The nominal capacity is 1.1 Ah.

Operating condition: The working history of this battery is just after formation. The working ambient temperature of this battery is 30 degrees Celsius. The cycling consists of four charging stages. In the first stage, the battery was charged at a constant current of 4.8 C to 20% state-of-charge (SOC). In the second stage, the battery was charged at a constant current of 5.2 C to 40% SOC. In the third stage, the battery was charged at a constant current of 5.2 C to 60% SOC. In the fourth stage, the battery was charged at a constant current of 4.16 C to 80% SOC until reaching 3.6 V. The battery was then discharged at a constant current of 4 C until reaching 2 V. The cycling state-of-charge of this battery ranges from 0% to 100%.

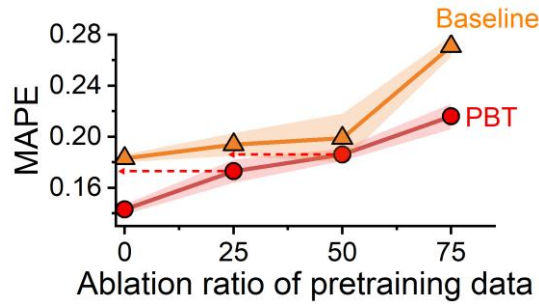
**Supplementary Figure 2. The unified prompt template for the LLM-based ageing embedder and one example.** a, the unified prompt template for the LLM-based ageing embedder. b, one example for one LiFePO<sub>4</sub>/Graphite 18650 cylindrical battery.



**Supplementary Figure 3. *t*-SNE visualization of prompt embeddings for the ageing conditions of training batteries generated by a large language model (LLM).** Colors represent datasets, and shapes indicate cathode materials. In general, embeddings of ageing conditions within each dataset cluster in similar regions, indicating that the LLM recognizes the influence of battery specifications on ageing behavior. Batteries within the same dataset typically share identical specifications—except for the Tongji and SNL datasets, which include multiple chemistries and formats—leading to more dispersed clustering. Within each dataset, the embeddings remain distinguishable, suggesting that the LLM also captures variations arising from operating conditions and formation protocols. Moreover, embeddings of ageing conditions sharing the same cathode tend to cluster closely even across datasets. These results demonstrate the LLM’s prior understanding of battery ageing mechanisms and its capacity to generate physically meaningful vector representations.



**Supplementary Figure 4. Battery life distributions across the 16 collected datasets.** The title of each subpanel reports the dataset name and summary statistics. *Std* denotes the standard deviation, and *n* is the number of batteries that reached end of life. For the CALB dataset, most cells did not degrade to 80% of nominal capacity; therefore, the cycle number at 90% capacity is used as the life label following BatteryLife<sup>1</sup>.



**Supplementary Figure 5. Model performance as a function of progressively reduced pretraining-data volume.** Shaded regions represent standard deviations across three independent runs. The arrowed red lines denote the performance of PBT under varying data-ablation ratios, shown for comparison with the baseline models trained with more pretraining data. The baseline is the PBT without BatteryMoE.

### Supplementary References

- 1 Tan, R. *et al.* in *Proceedings of the 31st ACM SIGKDD Conference on Knowledge Discovery and Data Mining V.2* 5789–5800 (Association for Computing Machinery, Toronto ON, Canada, 2025).
- 2 Zheng, H. *et al.* Learning from models beyond fine-tuning. *Nature Machine Intelligence* 7, 6-17 (2025). <https://doi.org/10.1038/s42256-024-00961-0>
- 3 Loshchilov, I. & Hutter, F. in *7th International Conference on Learning Representations, ICLR 2019, May 6, 2019 - May 9, 2019*. (International Conference on Learning Representations, ICLR).
- 4 Ba, J. L. Layer normalization. *arXiv preprint arXiv:1607.06450* (2016).
- 5 Zhang, H. *et al.* Battery lifetime prediction across diverse ageing conditions with inter-cell deep learning. *Nature Machine Intelligence* (2025). <https://doi.org/10.1038/s42256-024-00972-x>
- 6 Dai, D. *et al.* in *62nd Annual Meeting of the Association for Computational Linguistics, ACL 2024, August 11, 2024 - August 16, 2024*. 1280-1297 (Association for Computational Linguistics (ACL)).